Method to Measure the Moon using a Mass of a Mere Milligram

Ociepka, Oscar

Method to Measure the Moon using a Mass of a Mere Milligram

THESIS

submitted in partial fulfillment of the
requirements for the degree of

BACHELOR OF SCIENCE
in
PHYSICS

Author :	Oscar Ociepka
Student ID :	s2669684
Supervisor :	Prof.dr.ir. T.H. Oosterkamp
	Dennis Uitenbroek MSc
2^{nd} corrector :	Prof.dr. H.V.J. Linnartz

Leiden, The Netherlands, July 6, 2023

Method to Measure the Moon using a Mass of a Mere Milligram

Oscar Ociepka

Huygens-Kamerlingh Onnes Laboratory, Leiden University
P.O. Box 9500, 2300 RA Leiden, The Netherlands

July 6, 2023

Abstract

This experiment explored the sensitivity of a small magnet called the Zeppelin levitated using Meissner levitation in a superconductive trap within a cryostat. All six of the Zeppelin's rotational and vibrational modes were observed and quantified. Attempts were made to detect lunar patterns in the data with the aid of a simulation, but the noise levels hindered conclusive findings. Improvements to vibration isolation, including a lead damping block and a redesigned mass-spring system tested by a COMSOL simulation, significantly enhanced mode characteristics, most notably facilitating a frequency stability of one part per billion, taking a step towards quantum-scale ultrasensitive gravitational force sensors with further advancements in setup and analysis methods.

Contents

Chapter 1

Introduction

In the fascinating realm of quantum mechanics, objects can exhibit extraordinary behaviors that defy our everyday experiences. One captivating phenomenon is superconductivity, where certain materials can conduct electricity with near-zero resistance at extremely low temperatures. Exploiting this remarkable property, we can achieve Meissner levitation, a state in which objects can essentially float. In this experiment, we focus on levitating a small rotationally asymmetrical magnet called the Magnetic Zeppelin, clocking in at just under half* a milligram, using the power of superconductivity.

The experimental setup involves placing the Zeppelin in an elliptical well-shaped trap, made of tantalum, which is a superconductor at low temperatures. The trap is connected to a mass-spring system, and the entire apparatus is housed within a carefully controlled cryostat that reaches temperatures as low as 10 mK. This cryogenic environment combined with the mass-spring system not only provides excellent isolation from vibrations but also enables precise measurements of the Zeppelin's movement in its six rotational and vibrational degrees of freedom (modes). To accomplish this, we employ a sensitive read-out device called a Superconducting Quantum Interference Device (SQUID). The remarkable aspect of our experiment is our ability to determine the frequencies of these modes with an impressive precision of up to one part per billion.

While this setup has extremely broad applications, our specific aim is to explore the effects of the Moon's tidal forces on the Zeppelin within the context of Meissner levitation. The experiment presents a unique opportunity to investigate how tidal forces, caused by the gravitational pull of celestial bodies such as the Moon, can influence the levitation of the mag-

*The title of this thesis is, indeed, slightly misleading.

net. Whereas our ultimate goal is to establish the Zeppelin-trap system as an extremely sensitive force sensor, measuring the impact of tidal forces on the levitation height would be an important demonstration of its capabilities, especially over long periods of time, considering the long periodicity of the Moon.

By shedding light on the gravitational interaction between objects at increasingly smaller scales, our findings could eventually contribute to our understanding of fundamental physics and potentially pave the way for future advancements in various scientific and technological domains. It is through endeavors like these that we expand our knowledge and inch closer to unraveling the mysteries of the universe, bringing us closer to a comprehensive understanding of the fascinating interplay between general relativity and quantum mechanics, and perhaps, in a far future, a Theory of Everything.

Chapter 2

Theory

The theory section of this thesis provides a comprehensive understanding of the fundamental principles and concepts that underpin the experimental setup and observations in the subsequent sections. The aim is to establish the Zeppelin-trap system as an ultra-sensitive force sensor capable of detecting and quantifying minute forces. To achieve this, we delve into the Meissner levitation phenomenon, the role of Superconducting Quantum Interference Devices (SQUIDs) for read-out, and the influence of factors such as tidal forces on the levitation height and frequency of the Zeppelin.

Meissner levitation arises from the expulsion of magnetic flux by a superconducting material in the presence of an external magnetic field. The interaction between the Zeppelin and the image dipoles generated by the superconducting trap leads to its levitation. However, the levitation height of the Zeppelin is not solely determined by the Meissner effect. External forces, including tidal forces resulting from the gravitational attraction of celestial bodies on Earth, can also impact the Zeppelin's position within the trap.

The detection and measurement of these minute forces rely on the utilization of SQUIDs in the read-out system. SQUIDs are highly sensitive devices capable of detecting and quantifying small magnetic fields. The SQUID-based read-out system, in combination with harmonic oscillators, enables the conversion of magnetic flux changes into position or force measurements. This conversion capability allows for the precise monitoring and analysis of the Zeppelin's behavior.

While the focus of this thesis is to establish the Zeppelin-trap system as a sensitive force sensor, the influence of tidal forces serves as a convenient test for its capabilities. By monitoring the levitation height and frequency shifts resulting from tidal forces, we can demonstrate the high sensitiv-

ity and precision of the system in detecting and quantifying small forces. However, it should be noted that the application of the Zeppelin-trap system extends beyond the measurement of tidal forces and holds significant potential in various scientific and technological domains.

By providing a comprehensive theoretical foundation for the Zeppelin-trap system, this theory section establishes the groundwork for the subsequent analysis and interpretation of the experimental results presented in the methods and results sections of this thesis.

2.1 Meissner levitation

In this section, we will explore the fundamental principles underlying the phenomenon of Meissner levitation. We will discuss the concept of superconductivity and its role in expelling magnetic flux from a superconducting material when subjected to an external magnetic field. This expulsion of magnetic flux creates image dipoles, resulting in a repulsive force that enables the levitation of the magnetic Zeppelin within the superconducting trap. We will also emphasize that the restoring force for the levitation is gravity, which provides stability to the system. By understanding the mechanisms of Meissner levitation and the interplay between magnetic flux, image dipoles, and gravity, we can gain insights into the dynamics of the Zeppelin within the trap.

2.1.1 Superconductivity

Superconductors are materials that exhibit the remarkable property of near-zero electrical resistance below a critical temperature, denoted as T_c. At temperatures below T_c, the behavior of electrons in the material undergoes a remarkable transformation, forming Cooper pairs and enabling the flow of electrical current without any dissipation of energy. This is a result of Bardeen-Cooper-Schrieffer theory which is valid for pure metals, as will be used in our experiments.

The superconducting state is also characterized by a critical magnetic field, denoted as B_c. This critical field represents the maximum magnetic field that a superconductor can withstand while maintaining its superconducting properties. Above this critical field, the material transitions to a normal resistive state, losing its zero-resistance behavior.

2.1.2 Types of superconductors

Superconductors can be broadly classified into two categories based on their response to magnetic fields: Type I and Type II superconductors. Whilst both types have a single critical temperature T_c, Type I superconductors have a single critical field, B_c, below which they exhibit perfect diamagnetic behavior. Diamagnetism refers to the property of a material to generate an opposing magnetic field in response to an applied magnetic field, resulting in the expulsion of magnetic field lines from the interior of the superconductor. However, when the applied magnetic field exceeds B_c, Type I superconductors undergo an abrupt transition to the normal resistive state.

Type II superconductors, on the other hand, exhibit a more complex behavior in the presence of magnetic fields. They have two critical fields: the lower critical field, B_{c1}, and the upper critical field, B_{c2}. Below B_{c1}, Type II superconductors behave similarly to Type I superconductors, expelling magnetic field lines and exhibiting perfect diamagnetism. However, as the magnetic field increases and surpasses B_{c1} but remains below B_{c2}, Type II superconductors enter a mixed state known as the vortex state. In this state, tiny magnetic flux vortices penetrate the material, allowing Type II superconductors to maintain their superconducting state even in the presence of magnetic fields (Figure 2.1).

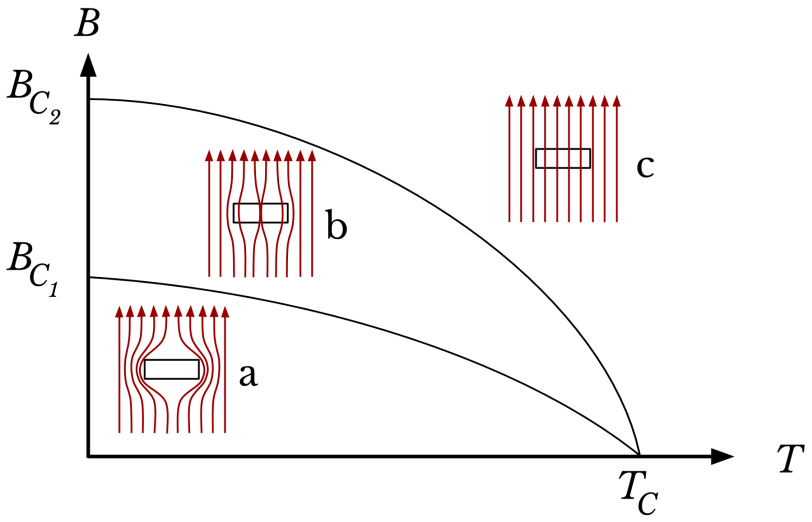

Figure 2.1: *Transition diagram of a Type-II superconducting metal block. For a Type I superconductor, B_{c1} and B_{c2} coincide. Image retrieved.[1]*

Understanding the critical temperature, T_c, and critical magnetic field, B_c, characteristics of superconductors is essential for comprehending the subsequent discussions on the different behaviors exhibited by Type I and Type II superconductors. These critical parameters play a crucial role in the phenomenon of Meissner levitation and its application to the Zeppelin within the superconducting trap.

2.1.3 Eddy currents

Eddy currents are circulating currents induced in a conductor when it is exposed to a changing magnetic field. They are a direct consequence of Faraday's law of electromagnetic induction, which states that a changing magnetic field through a conductor induces an electromotive force (EMF) that gives rise to an electric current. Mathematically, Faraday's law can be expressed as:

$$\epsilon = -\frac{d\Phi}{dt} \tag{2.1}$$

where ϵ represents the induced EMF and Φ denotes the magnetic flux through the conductor.

In the context of superconductivity, eddy currents hold a special significance. When a superconductor is subjected to a changing magnetic field, its remarkable property of zero electrical resistance prevents the generation of conventional resistive currents. Instead, the magnetic field induces circulating currents within the superconductor itself, known as superconducting or persistent currents. These persistent currents flow indefinitely without any dissipation of energy, creating a unique behavior distinct from normal conductors.

The presence of eddy currents in superconductors is a crucial aspect in various applications. In Meissner levitation, for instance, the expulsion of magnetic field lines from the interior of the superconductor is primarily achieved by the formation of persistent currents, resulting in the phenomenon of perfect diamagnetism. This remarkable characteristic allows superconductors to exhibit strong repulsion to magnetic fields, leading to their ability to levitate in the presence of a magnetic trap.

2.1.4 Image dipoles

When a magnetic or electric dipole is placed near a superconducting surface, it induces an image dipole within the conductor due to the redistribution of charges (Figure 2.2). This image dipole acts as a mirror reflection

of the original dipole, with opposite polarity, and results in an attractive or repulsive force between them. In the context of our experiment, the Zeppelin, acting as a magnetic dipole, interacts with the conducting trap through the phenomenon of image dipole interaction. The presence of the superconducting trap causes the Zeppelin's image dipoles to be repelled from the trap, exerting a force that contributes to the levitation effect.

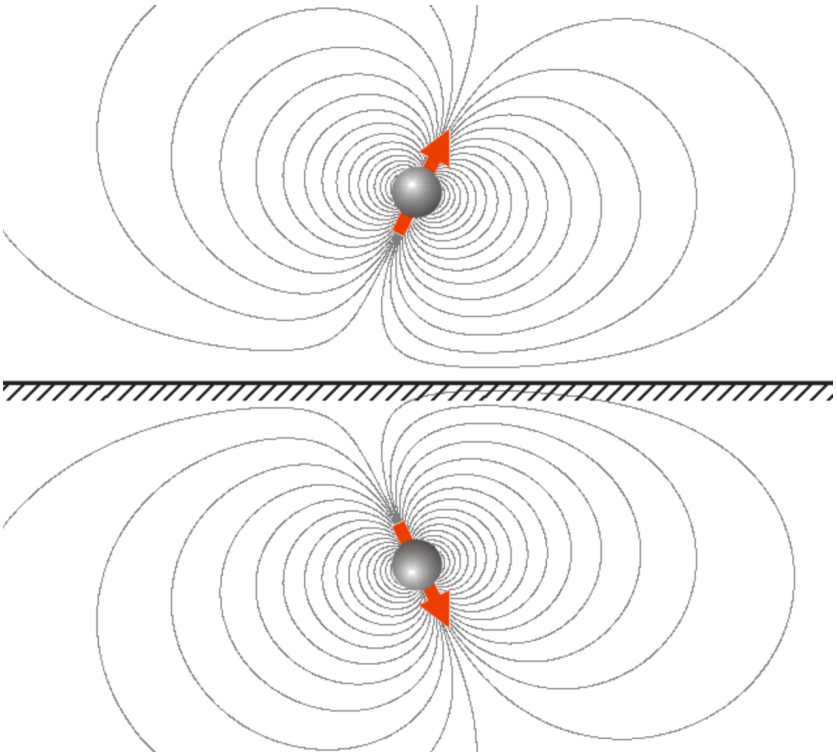

Figure 2.2: *Schematic of magnetic image dipole interaction, where the horizontal surface is a superconductor. The top dipole represents a real magnet such as the Zeppelin, the bottom its image dipole. Image retrieved.[1]*

Quantifying this dipole interaction is crucial for determining the levitation height, which is dependent on the dipole interaction energy and the gravitational potential, and thereby the theoretical oscillation frequency of the six rotational and vibrational modes.

Using the image method, the repulsion between the Zeppelin and the conducting trap can be quantified as the interaction between two dipoles. The magnetic dipole $\overrightarrow{m}_1$ generates a magnetic field $\overrightarrow{B}(r)$:

$$\overrightarrow{B}(r) = \frac{\mu_0}{4\pi}\left(\frac{3(\overrightarrow{m}_1 \cdot \hat{r})\hat{r} - \overrightarrow{m}_1}{r^3}\right) + \frac{2\mu_0}{3}\overrightarrow{m}_1\delta^3(r) \tag{2.2}$$

The interaction energy for the dipole interaction between the Zeppelin's dipole $\overrightarrow{m}_1$ and its image dipole $\overrightarrow{m}_2$ is given by:[5]

$$U_d(r) = -\frac{1}{2}\overrightarrow{m}_2 \cdot \overrightarrow{B}(r) \tag{2.3}$$

where the factor $\frac{1}{2}$ stems from $\overrightarrow{m}_2$ being an image dipole in a superconductor in which there is no magnetic field. Evaluating this then yields the expression for dipole interaction energy, where the $\delta^3(r)$ term vanishes as the dipoles cannot coincide exactly:

$$U_d(r) = -\frac{\mu_0}{8\pi}\left(\frac{3(\overrightarrow{m}_1 \cdot \hat{r})(\overrightarrow{m}_2 \cdot \hat{r}) - \overrightarrow{m}_1 \cdot \overrightarrow{m}_2}{r^3}\right) \tag{2.4}$$

2.1.5 Restoring force

In order to establish an equilibrium between the dipole interaction and a restoring force, a counteracting force is required. In the case of the Zeppelin's levitation, gravity serves as the restoring force. The gravitational potential (U_g) can be expressed as:

$$U_g(z) = mgz$$

where m is the mass of the Zeppelin and g is the acceleration due to gravity. The gravitational potential arises from the interaction between the Zeppelin's mass and the gravitational field. By balancing the dipole interaction energy and the gravitational potential, an equilibrium position can be achieved. This ensures that the Zeppelin remains suspended in the trap, with the gravitational force opposing the dipole interaction force. Thus, gravity acts as the restoring force, allowing the Zeppelin to maintain its levitated state within the trap.

2.1.6 Equilibrium position

The levitation height of the Zeppelin can be determined by analyzing the total potential energy of the system. The total potential energy is the sum of the gravitational potential energy $U_g(z)$ and the dipole interaction energy $U_d(r)$. By differentiating the total potential energy with respect to z and setting it equal to zero, we can find the equilibrium position or the levitation height. Mathematically, this can be expressed as:

$$\frac{d}{dz}(U_g(z) + U_d(z)) = 0 \tag{2.5}$$

Solving this equation for z will give us the value of z at which the Zeppelin reaches a stable levitation height. This approach allows us to determine the precise positioning of the Zeppelin within the trap, ensuring that it remains suspended at a specific height above the superconducting material.

Using the gravitational potential and the dipole interaction energy found earlier, and making use of the geometry of the system, defining a rotational angle β of the Zeppelin along its longitudinal axis, along with trigonometric manipulation under the assumption that the magnet is a single point dipole, the total potential U_z is found to be:

$$U_z = U_g(z) + U_d(z) = mgz + \frac{\mu_0 \left|\overrightarrow{m}_1\right| \left|\overrightarrow{m}_2\right|}{64\pi z^3}(1 + \sin^2(\beta)) \tag{2.6}$$

Differentiating as expressed in Equation 2.5 above, solving for the levitation height $z = z_0$ and substituting $\left|\overrightarrow{m}_1\right| = \left|\overrightarrow{m}_2\right| = B_r V/\mu_0$ with B_r the remanence magnetic field of the Zeppelin and V its volume, yields the expression for its equilibrium position in z:

$$z_0 = \left(\frac{3B_r^2 V^2}{64\pi\mu_0 mg}\right)^{\frac{1}{4}} \tag{2.7}$$

Here it was assumed that $|\beta| \ll 1$, since $\beta = 0$ describes the equilibrium in β.

The equilibrium position in x and y is trivial, as the trap and the Zeppelin are symmetric in these directions, which means the driving and restoring forces are equal and opposite dipole interactions, implying an equilibrium position in the middle of the trap.

2.1.7 Spring constants

The expression for the total potential U_z allows us to define spring constants k_z and κ_β corresponding to the z mode and the β mode, respectively, by using the potential energy of a harmonic oscillator, as follows:

$$k_z = -\frac{dU_z^2}{dz^2}|_{z=z_0} = \frac{3B_r^2 V^2}{16\pi\mu_0 z_0^5} \tag{2.8}$$

Once again, it was assumed that $\beta \ll 1$. The equation for β reads:

$$\kappa_\beta = -\frac{dU_z^2}{d\beta^2}|_{z=z_0,\,\beta=0} = \frac{3B_r^2 V^2}{32\pi\mu_0 z_0^3} \tag{2.9}$$

The frequency at which the z and β modes oscillate can now easily be found by solving for the harmonic oscillation angular frequencies ω_z and ω_β:

$$\omega_z = \sqrt{\frac{k_z}{m}} \tag{2.10}$$

with m the mass of the Zeppelin, and

$$\omega_\beta = \sqrt{\frac{k_\beta}{I}} \tag{2.11}$$

with I the moment of inertia of the Zeppelin, the equivalent of mass for rotational angular frequencies.

The same method can be applied to the four other modes, resulting in expressions for the spring constants k_x, k_y, κ_α, and κ_γ. The situation is different, however, as the restoring force will be another dipole interaction force, resulting in a different total potential. Quadrupole interactions can also be taken into account for more precise expressions. Seen as the k_z and κ_β spring constants are most strongly dependent on levitation height and suffice for quantifying the influence of the tides, though, the calculation of the four remaining spring constants is omitted.

2.2 SQUID readout

The SQUID (Superconducting Quantum Interference Device) readout is a crucial component in our experimental setup for measuring the oscillation frequencies of the magnet. The SQUID operates based on the principle of detecting extremely small changes in magnetic fields through the interference of superconducting currents. It offers high sensitivity and precision in capturing the magnetic signals generated by the magnet's motion.

To ensure accurate measurements, the SQUID readout system undergoes careful calibration procedures. This calibration process establishes the relationship between the detected magnetic field and the corresponding physical quantities, such as the magnet's oscillation amplitude and phase. Precise calibration allows us to accurately interpret the SQUID signal and extract meaningful data.

Furthermore, the quality of the measurement modes in the SQUID readout is of paramount importance. Mode quality refers to the ability of the system to detect and distinguish different oscillation modes of the magnet with high fidelity. Achieving high mode quality ensures that we can capture the unique features and characteristics of each oscillation

mode, providing valuable insights into the behavior of the system under different conditions.

In the following subsections, we will delve deeper into the principles of SQUID readout, the calibration procedures employed, and the evaluation of mode quality to obtain reliable and accurate measurements of the magnet's oscillation frequencies.

2.2.1 Principle

The principle of SQUID (Superconducting Quantum Interference Device) readout is a fundamental aspect of our experimental setup, enabling precise measurements of the magnet's position and its corresponding oscillation modes. The SQUID readout system operates on the principle of electromagnetic induction along with flux quantization. As the asymmetrical magnet attached to the Zeppelin oscillates, it induces a time-varying magnetic flux through a detection coil (Figure 2.3). This changing flux is then detected by the SQUID itself, a highly sensitive device that exploits the quantized behavior of superconducting loops.

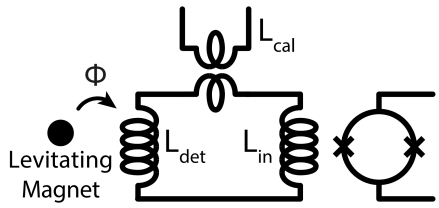

Figure 2.3: *Schematic of the levitating magnet (Zeppelin) next to the SQUID readout system. The figure shows the relevant calibration, detection and SQUID input coils along with their respective corresponding inductances L_{cal}, L_{det}, and L_{in}. The rightmost component is the SQUID itself. (Uitenbroek, 2021).[2]*

The SQUID reacts to the changing magnetic flux by generating a voltage proportional to the rate of change of the magnetic flux. This voltage response is known as the SQUID output voltage, which can be measured and recorded. By analyzing the SQUID voltage, we can extract information about the position and motion of the magnet. Specifically, the SQUID voltage is directly dependent on the magnet's position in every mode with different calibration factors, providing us with a means to translate between the SQUID output voltage and the mode oscillation.

2.2.2 Calibration

Calibration plays a critical role in our experiment as it allows us to establish the relationship between the measured voltage signal and the corresponding motion of the Zeppelin. The calibration process involves determining the sensitivity, which is the conversion factor between the measured voltage and the displacement and angular tilt of the Zeppelin.

To calibrate the system, we utilize a magnetic drive. The calibration coil generates a magnetic flux, which induces a current and, consequently, a flux in the pickup coil and the SQUID input coil. The flux in the pickup coil influences the oscillation of the magnet, and this response can be used to measure the energy coupling between the Zeppelin and the circuit along each mode.

The energy coupling represents the ratio between the energy stored in the electrical system and the kinetic energy of the oscillating magnet. It quantifies the efficiency of energy transfer between the two systems. The coupling is independent for each resonance frequency.

During calibration, it is essential to determine the energy coupling experimentally. The coupling β^2 is expressed as the fraction of energy in the electrical system E_{system} to the kinetic energy of the magnet E_{kin}. The electrical system's energy includes contributions from the pickup coil, SQUID input coil, calibration coil, and possible resistance in the wires, whereas the kinetic energy of the magnet is found by assuming harmonically oscillating modes. The coupling reads:

$$\beta^2 = \frac{E_{\text{system}}}{E_{\text{kin}}} = \left(\frac{d\Phi}{dx}\right)^2 \frac{1}{L_{\text{tot}} m\omega^2} \tag{2.12}$$

where Φ represents the flux, L_{tot} the total inductance, m the mass of the Zeppelin and ω the relevant angular frequency. With this coupling, we can find the conversion factor for the sensitivity of the SQUID, by utilizing the responsivity equation:[7]

$$\frac{dU}{dx} = -\frac{M}{L_{\text{tot}}} V_\Phi \frac{d\Phi}{dx} = -\frac{M}{L_{\text{tot}}} V_\Phi \sqrt{\beta^2 L_{\text{tot}} m\omega^2} \tag{2.13}$$

where we introduced a mutual inductance M and a SQUID gain V_Φ. A more detailed derivation can be found in (Uitenbroek, 2021).[2]

By calibrating the system and determining the appropriate conversion factor, we can accurately relate the measured voltage signals from the SQUID to the corresponding displacement of the Zeppelin. This enables us to quantify the motion and physical properties under investigation, and attach a quantification to the quality of the modes.

2.2.3 Mode quality

Now that we can determine the position of the Zeppelin over time, we can assess the quality of the mode in two main ways. These measures allow us to evaluate the performance and sensitivity of the system.

Firstly, the Q factor, also known as the quality factor, plays a crucial role. It includes the decay time of the mode and indicates the mode's ability to sustain oscillations. A higher Q factor corresponds to a longer decay time, signifying a higher quality mode. This is desirable as it enables the system to measure tiny forces with greater precision and accuracy, because a high Q factor implies low damping of the mode. The Q factor is found by:

$$Q = \frac{1}{2}\omega_0 \tau \tag{2.14}$$

where τ, the decay time, is the time it takes for a driven mode to decay in amplitude by a factor e^{-1}. Note that this expression is valid only for high Q factors, as a correction factor for ω_0 is needed for high damping.

Secondly, the mode temperature is an important parameter to consider. It refers to the effective temperature of the mode and provides insights into its thermal behavior. A lower effective mode temperature implies that the mode experiences minimal fluctuations and remains relatively stable. This is advantageous as it reduces unwanted motion and ensures better control over the system. The mode temperature T_{mode} is found, by virtue of the equipartition theorem, from equating:

$$m\omega_0^2 \Delta x^2 = k_B T_{\text{mode}} \tag{2.15}$$

where Δx signifies the random motion of the modes. It should be noted that the interaction between the mode temperature and the Q factor introduces a trade-off: a very low mode temperature can be achieved from high damping, but this would decrease the Q factor and thereby defeat the purpose of a low mode temperature.

2.3 Tidal force effects

The interaction between celestial bodies, such as the Moon and the Sun, with the Earth gives rise to intriguing phenomena known as tidal forces. These forces, although relatively weak, exert an influence on our environment, including the gravitational acceleration g experienced by objects on Earth, which we normally take to be constant at 9.81 m s^{-2}. Consequently,

the levitation height of the Zeppelin in our experiment is altered, leading to changes in the effective spring constants that govern its oscillatory behavior. As a result, the frequencies of the z mode and the β mode, which we determine using our SQUID data, are also affected. In this subsection, we will explore the expressions for tidal forces, their impact on the levitation height, and how they influence the oscillation frequencies, providing valuable insights into the potential of our setup as a sensitive force sensor.

2.3.1 Tidal forces

Tidal forces emerge due to the gravitational interaction between celestial bodies and the Earth. These forces arise from the difference in gravitational pull experienced by different parts of the Earth that are closer or farther from the celestial body, effectively deforming the Earth into an ellipsoid (Figure 2.4). Tidal forces can be quantified by considering the gravitational acceleration variations caused by celestial bodies. The dominant contribution typically comes from the Moon due to its proximity to the Earth and its mass.

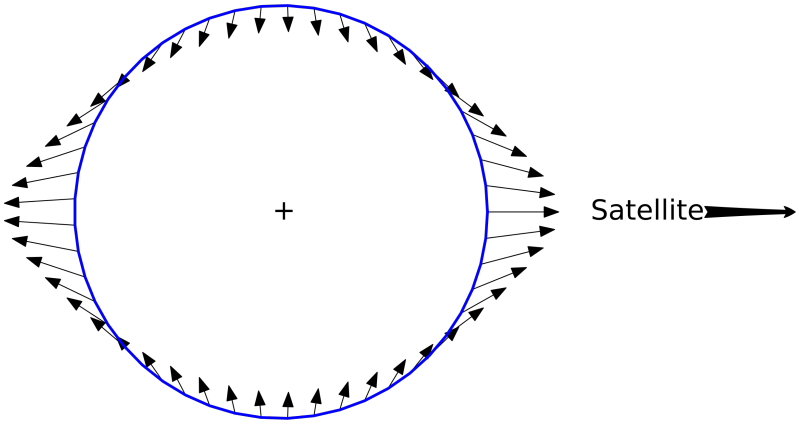

Figure 2.4: *Schematic of the influence of a satellite or celestial body, e.g. the Moon, on the gravitational field of the Earth. This is called the gravity differential field. Image retrieved.[1]*

The gravitational force exerted by the Moon, or by extension any celestial object, on the Earth can be approximated by Newton's law of universal gravitation:

$$\overrightarrow{F}_g = -\frac{GMm}{R^2}\hat{r} \tag{2.16}$$

where $\overrightarrow{F}_g$ represents the gravitational force, G is the gravitational constant, M denotes the mass of the Moon, m is the mass of the object on Earth, and R signifies the distance between the Moon and the object in question. Introducing a distance Δr between the object and the center of mass of the Earth, and dividing out the object mass m, yields a refined expression for the gravitational acceleration g:

$$\overrightarrow{g} = -\frac{GM}{(R \pm \Delta r)^2}\hat{r} \tag{2.17}$$

Taking the Maclaurin series expansion, under the assumption that $\Delta r \ll R$, and subtracting the original gravitational acceleration, results in an expression for the extremum change in gravitational acceleration Δg due to tidal forces of the Moon:

$$\Delta g = \pm 2\Delta r \frac{GM}{R^3} \tag{2.18}$$

The tidal correction force being a differential force, it is intuitive that it should scale as R^{-3}. Typical lunar tidal acceleration correction does not exceed $1.1 \cdot 10^{-7}$ gravitational accelerations (g), whereas solar effects are even smaller by a factor 0.45.

In the context of our experiment, we assume that tidal forces are the primary source of variation in gravitational acceleration. This assumption is based on several factors. Firstly, lunar tidal forces are generally the largest contributors to variations in the Earth's gravitational field, particularly due to the Moon's close proximity. The tidal force exerted by the Moon exhibits a larger magnitude compared to other celestial bodies. Secondly, the tidal forces have a distinct periodicity associated with the motion of the Moon and the Sun. These periodic variations are well-studied and can be precisely predicted. This periodicity is an advantage when taking a spectrum over large timescales, as it facilitates the detection by Fourier transform. Moreover, other unpredictable variations, for example due to turbulence in the Earth's mantle, are hardly distinguishable from noise; or they are relatively constant for monthly timescales, such as asymmetric mass distribution or equatorial bulging. Therefore, we consider tidal forces as the primary factor influencing the changes in gravitational acceleration. By measuring the corresponding oscillation frequencies of the Zeppelin under different tidal conditions, we can indirectly quantify the effect of tidal forces on the levitation height and the resulting modifications in the spring constants.

2.3.2 Influence on modes

As it has now been quantified how the gravitational acceleration g depends on the tidal forces, we connect this to the oscillation frequencies of the modes, so that they can be used as sensitive force sensors. To demonstrate this relationship rigorously, we pedantically redefine the total gravitational acceleration as experienced on Earth to be time-variant, denoted $g(t)$. This consists of a time-independent constant term g_0, and a small, time-dependent variation $\Delta g(t)$, as found in Equation 2.18, such that:

$$g(t) = g_0 + \Delta g(t) \tag{2.19}$$

Similarly, the measured oscillation frequency of a mode $f(t)$ is split as follows:

$$f(t) = f_0 + \Delta f(t) \tag{2.20}$$

where f_0 can be taken to be the mean of the measured oscillation frequency during some time interval, and $\Delta f(t)$ the difference to the mean. Now recall Equations 2.7, 2.8, 2.10, and the conversion between angular frequency ω and oscillation frequency f, namely $\omega = 2\pi f$. Substituting and solving for $f_z(t)$ yields an expression of the oscillation frequency in z in terms of $g(t)$:

$$f_z(t) = \aleph g(t)^{5/8} \tag{2.21}$$

where we defined a constant $\aleph$ for clarity:

$$\aleph \equiv \frac{1}{2\pi}\sqrt{\frac{3}{12\pi}}\left(\frac{64\pi}{3}\right)^{5/8}(B_r V)^{-1/4}(\mu_0 m)^{1/8} \tag{2.22}$$

Splitting in aforementioned way yields:

$$f_{z,0} + \Delta f_z(t) = \aleph(g_0 + \Delta g(t))^{5/8} \tag{2.23}$$

Taking the first-order Taylor expansion for $\Delta g(t) \ll g_0$ then gives two terms:

$$f_{z,0} + \Delta f_z(t) = \aleph g_0^{5/8} + \frac{5}{8}\aleph \Delta g(t) g_0^{-3/8} \tag{2.24}$$

where we recognize that the first term on the LHS is equivalent to the first term on the RHS by virtue of Equation 2.21, implying the following z mode oscillation frequency shift:

$$\frac{\Delta f_z(t)}{f_{z,0}} = \frac{5}{8}\frac{\Delta g(t)}{g_0} \tag{2.25}$$

The β mode oscillation frequency shift can be derived following the same procedure:

$$\frac{\Delta f_\beta(t)}{f_{\beta,0}} = \frac{3}{8}\frac{\Delta g(t)}{g_0} \tag{2.26}$$

Chapter 3

Methods

In the methods section, we present a detailed description of the experimental setup and techniques used in this research. We begin by introducing the cryostat, which provides a stable environment at ultra-low temperatures for our experiments, and enables superconductivity. We then discuss the details of the trap and Magnetic Zeppelin, including their design and construction.

Next, we focus on the mass-spring system that supports the Zeppelin within the trap. We explain the key parameters and materials used, as well as the considerations during assembly. We also highlight the simulations conducted to optimize the design of this system, ensuring its stability and minimizing unwanted influences.

Additionally, we address the simulations carried out to investigate the impact of tidal force gravity on our measurements. These simulations are necessary to evaluate whether the data from the Zeppelin can be interpreted as a force sensor of lunar gravity.

By providing a comprehensive overview of the cryostat, trap and Zeppelin setup, the mass-spring system, and the conducted simulations, this methods section offers a clear understanding of the experimental techniques employed in this study. These methodologies have proven crucial for obtaining accurate and reliable measurements.

3.1 Cryostat

Our cryostat, colloquially known as *Marshmallow*[*], plays a pivotal role in our experimental setup, as it provides the low temperature environment necessary for reducing thermal noise and enabling superconductivity. Achieving and maintaining extremely low temperatures is crucial for our measurements, as it allows us to minimize thermal vibrations and achieve the desired sensitivity and precision in our gravity experiments, whereas superconductivity is necessary for the Zeppelin to levitate in the first place.

Our cryostat is a dry dilution refrigerator. This refrigerator operates by circulating liquid nitrogen, helium-4 (^{4}He), and helium-3 (^{3}He) throughout the cryostat. To initiate the cooling process, liquid nitrogen is used for pre-cooling, taking advantage of its relatively low boiling point of 77 K. Subsequently, a mix of ^{4}He and ^{3}He, coupled with a pulse tube (PT), is employed to further cool the system. Unlike conventional wet dilution refrigerators, the dry dilution refrigerator utilizes the PT to circulate ^{4}He in a closed cycle, eliminating the need for cooling baths.

During the PT cycles, the compressed and decompressed ^{4}He undergoes a thermodynamic process, extracting energy from the system. The PT operates at a frequency of 1.4 Hz, the harmonics of which become discernible in the SQUID data, being one of the main reasons to improve the vibration isolation within the cryostat.

The PT connects to the first two plates in the Outer Vacuum Chamber (OVC), known as the 50K and 4K-plates. However, achieving even lower (mK) temperatures necessitates the dilution of ^{4}He with ^{3}He, which takes place in a closed system called the mixing chamber situated within the Inner Vacuum Chamber (IVC). In the mixing chamber, a mixture of ^{4}He and ^{3}He is present, with the phases separated into concentrated and dilute phases. The dilute phase, consisting of approximately 6% ^{3}He and 94% ^{4}He, resides below the concentrated phase, which predominantly comprises ^{3}He. A phase boundary separates these two phases. Through the dilution process, where ^{3}He moves from the concentrated phase to the dilute phase across the phase boundary, energy is extracted from the surroundings. The ^{3}He subsequently evaporates in the distillation chamber (still) and undergoes recycling within the system, perpetuating the cooling process by effectively removing energy and heat.

[*]Cold as they are, cryostats in the Oosterkamp group were traditionally named after snowmen: the "Yeti" was first, then the "Olaf" and the "Marshmalllow" followed, named after characters from Disney's *Frozen*. This pattern might prove short-lived, though, as the consensus on the name of the new cryostat is tending towards "Elsa".

The effective result of combining these cooling methods is a plate system where multiple plates are stacked above each other, separated by thermally isolating material, where each plate is colder than the plate above it. In order of warm to cold, there is the room temperature plate (RT-plate), the 50K-plate, the 4K-plate, the 1K-plate (or still plate), the 50mK-plate, and the 10mK-plate (or mixing chamber plate) (Figure 3.1). Our experiment is thermally connected to the coldest plate. In practice, this 10mK-plate may experience difficulties cooling, sometimes not even dropping below 100mK, mainly due to heat dissipation.

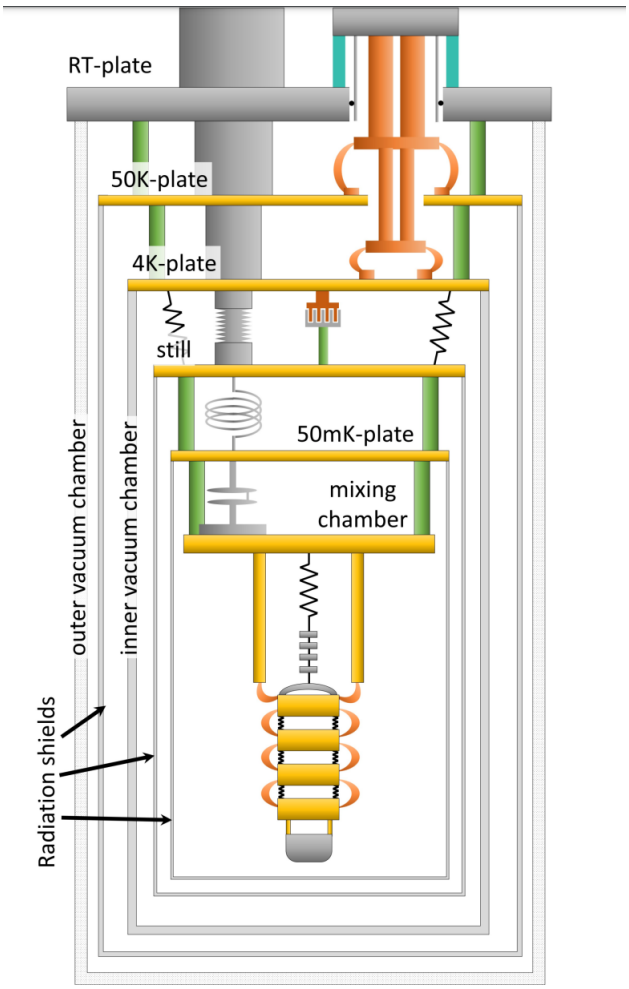

Figure 3.1: *Schematic of the plate system of the cryostat with all its plates. The mass-spring system of our experiment deviates slightly from the figure, though the principle that the experiment is thermalized to the mixing chamber plate is the same. (De Wit, 2019).[6]*

Due to the vacuum environment, heat extraction from the experimental setup is limited, as convection is absent. To ensure cooling reaches the experiment, copper ribbons are utilized to conduct heat. These ribbons are connected to the mixing chamber plate, which experiences the most effective cooling, and extend to the housing of the experiment. The copper at all connections was properly sanded and cleaned with ethanol for better thermalization. Bends in the ribbons prevent the formation of bypasses for vibrations, ensuring optimal thermal conduction without introducing additional disturbances (Figure 3.2).

Creating a vacuum is crucial for accurate gravity measurements, as gravity is a weak force that can be easily dominated by noise caused by excessive air pressure. Therefore, it is essential to decrease the pressure to a level where drag becomes negligible. A vacuum is achieved both in the OVC and the IVC, with the vacuum in the IVC considered to be an ultra-high vacuum. This is achieved through the use of various pumps, starting with a large pump that handles the initial high volume and followed by specialized pumps like a turbo pump to achieve higher vacuums.

To minimize any motion that may affect the measurements, it is crucial to inhibit the movement of the setup. Since the SQUID is capable of highly sensitive measurements, even small motions of the trap can interfere with the gravity measurements. Therefore, exceptional vibration isolation is implemented to prioritize accurate gravity measurements rather than measuring vibrations. The cryostat is situated on a measurement island, suspended from a large tripod that rests on dampers. This configuration effectively reduces vibrations generated in the immediate vicinity of the cryostat. The measurement island consists of a 25-ton concrete block placed on dampers, providing an initial level of isolation. However, given the substantial strength of vibrations that can still reach the cryostat, particularly from equipment located above it (with the pulse tube being the primary source), additional vibration isolation measures are implemented within the cryostat itself. These measures include the use of springs placed between the plates, as well as a sophisticated multi-stage mass-spring system designed to isolate the experiment further from the vibrations in the rest of the cryostat.

By employing a dry dilution refrigerator, incorporating the mixing chamber, utilizing copper ribbons for heat conduction, establishing a vacuum environment, and implementing vibration isolation measures, our experimental setup ensures optimal thermal conditions and minimizes unwanted disturbances, enabling precise and accurate gravity measurements.

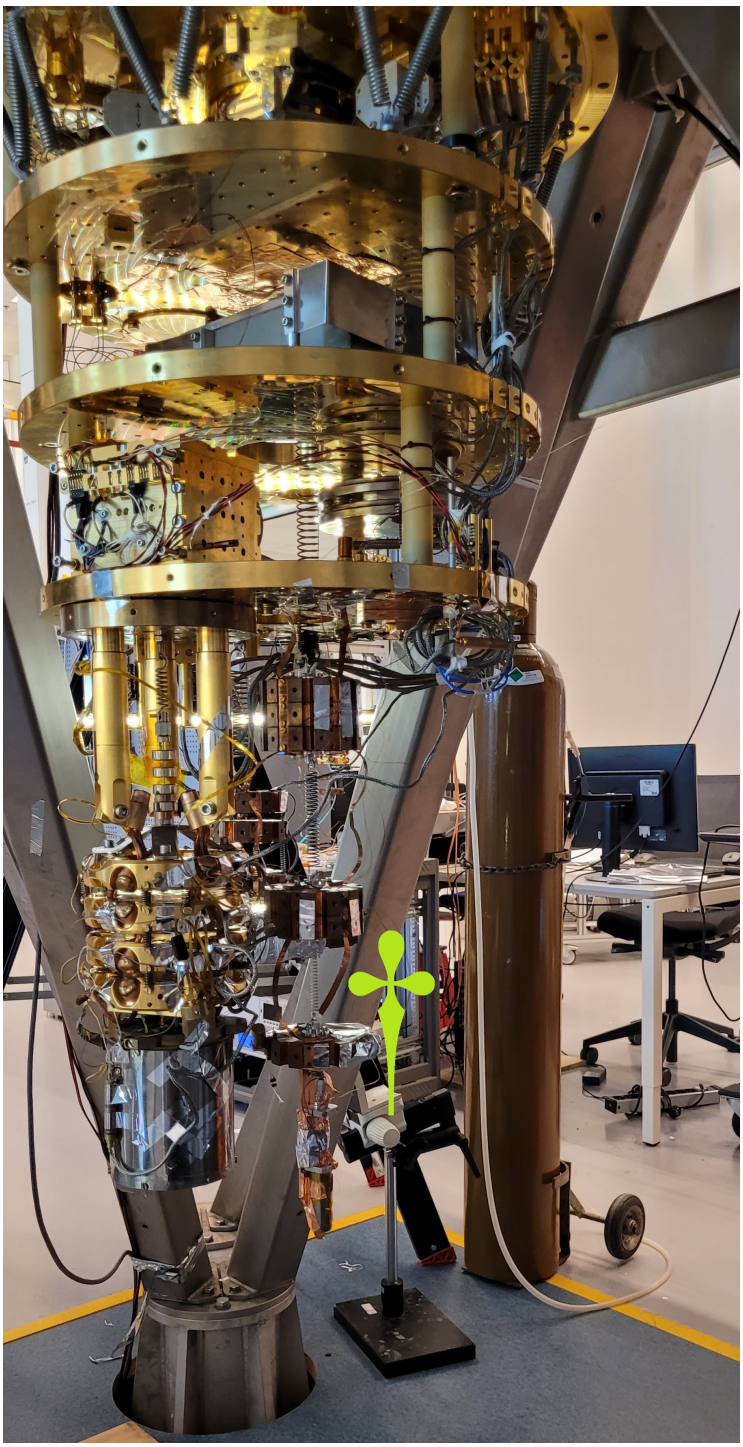

Figure 3.2: *Photograph of the cryostat without its shields. The mixing chamber plate, 50mK-plate, still plate and 4K-plate are visible. The lime dagger indicates the position of the mass-spring system, with its thermalizing copper ribbons.*

3.2 Zeppelin-trap system

At the core of our experiment lies the Zeppelin-trap system, a carefully designed ultra-sensitive mechanical resonator. The system consists of a Magnetic Zeppelin, which is the object that is levitated, and a superconducting well-shaped trap that generates electromagnetic fields to limit its motion in all degrees of freedom. Housed within a dedicated structure, the Zeppelin-trap system is the smallest yet most fundamental component of the entire setup, profiting from the exceptional vibration isolation around it, enabling it to be sensitive to gravitational vibrations. This section explores the build of the Zeppelin-trap system, highlighting the importance of its specifications in our experiments.

3.2.1 Magnetic Zeppelin

The Magnetic Zeppelin, or Zeppelin[†] for short, is the tiny object which ultimately serves as the gravitational force detector. It consists of three cubic magnets in a row and a roughly equally large glass bead, the magnets and the bead being held together with glue (Figure 3.3).

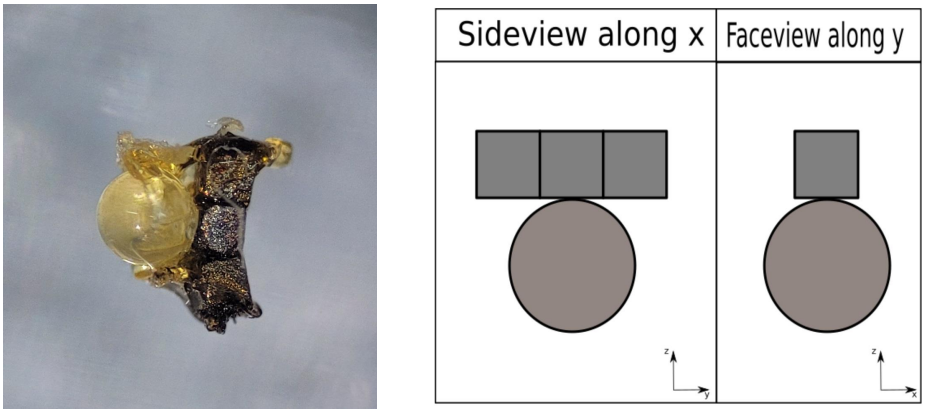

Figure 3.3: *Schematic and microscopic picture of the Magnetic Zeppelin. (Van Halteren, 2022).[3]*

[†]Originally, the setup consisted of a superconducting ball in a magnetic well. The levitating ball was made of lead, inviting the name "Lead Zeppelin". The setup developed past this stage, but the usage of "Zeppelin" for the levitating particle stuck around.

The magnets are cubes with side lengths of 0.25 mm, made of N50 Rare Earth Neodymium (NdFeB), coated with a non-superconducting nickel-copper-nickel coating of roughly 20 μm thick. The magnets were etched to remove some of the coating. The resulting thinner coating causesa decrease in eddy current damping, due to the lower volume of resistive material. The three cubes are placed in a row so as to introduce a longitudinal direction and thereby break the otherwise present rotational symmetry, which is useful for splitting the modes. However, three magnets in a row are still easily rotationally symmetric along their longitudinal axis, prompting the addition of the non-magnetic glass bead, which serves as additional weight and a clear separation of all the modes. Altogether, the total mass is estimated 0.4 mg.

During one moment in which the cryostat was nonoperational, a substantial amount of glue was placed around the magnets. This procedure was a reaction to an observation: upon inspection under a microscope, the magnets of the Zeppelin seemed to have small, hair-like threads sticking out in all directions. These threads were suspected to be magnetic; a result of the aforementioned coating, thereby possibly introducing nonlinearities to the system as they moved, or other unpredictable negative effects on the observed behavior of the Zeppelin. The glue is meant to subdue the movement of these threads, improving the quality of the Zeppelin. New magnets with non-magnetic coating have been purchased as well, for future use.

3.2.2 Trap and housing

The well-like object which constrains the Zeppelin is accordingly called the trap. The trap is made of tantalum, a Type-I superconductor with a critical temperature of 4.8 K. It is elliptical in the x-y plane, and straight in the z direction, with a semi-major axis of 2.3 mm and an eccentricity of 0.63 (Figure 3.4). The trap comes with a lid with holes, which are there for air to escape as necessary for a vacuum, and for wiring to pass through.

The trap was chosen elliptical for familiar reasons: to break the symmetry, enabling superior mode separation. More specifically, the elliptical shape separates the x vibrational mode from the otherwise comparable y mode. In this way, the combination of the asymmetrical design of the Zeppelin with the elliptical shape of the trap facilitates an incredible distinguishability between modes, forming a solid foundation for our experiment.

The trap-Zeppelin system is placed in an aluminium housing, together

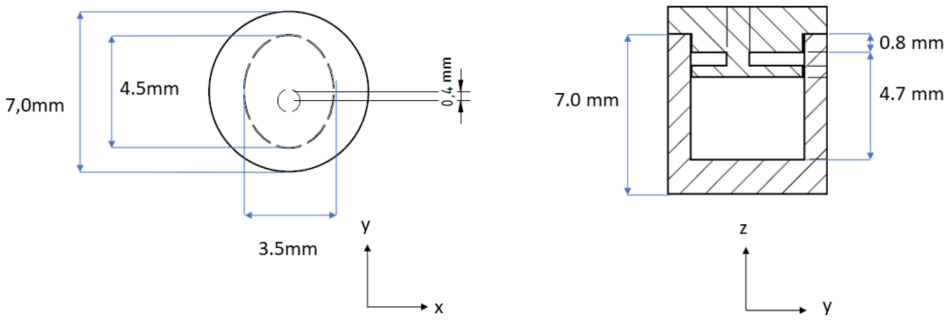

Figure 3.4: *Dimensions of the trap in the x-y plane and in the y-z plane. (Uitenbroek, 2021).[2]*

with the SQUID wiring which is also shielded with niobium. As both these pure metals are superconductors at millikelvin temperatures (Al is Type-I, Nb is Type-II), they are excellent shields for the Zeppelin against magnetic field influence from outside the trap. This housing is placed in a copper clamp and subsequently attached to the lowest mass of the mass-spring system in the cryostat.

3.3 Mass-spring system

If the trap-Zeppelin system is the core of the experiment, then the mass-spring system is the engine: it is the mass-spring system that enables the Zeppelin to measure at the precision it does, by damping as many vibrations from the surrounding as possible.

The mass-spring system unsurprisingly consists of multiple different copper masses connected by stainless steel springs with varying spring constants. The top mass is attached in some fashion to a plate of the cryostat, though not thermalized to it, and the remaining springs and masses hang to each other by hooks. Each hook is surrounded by either nylon tape or similar soft plastic, to prevent sudden slip motions which would harm the measurements. All masses are thermalized to the mixing chamber plate. This is necessary, as the springs themselves insulate heat, whereas the bottom mass with the trap-Zeppelin system must be as cold as possible to minimize thermal vibrations and enable superconductivity. The top mass also houses a piezo element to generate vibrations to stimulate the modes.

It should be noted that the length and spring constant specifications of

springs change significantly at millikelvin temperatures. Steel springs can contract up to 15% in length between room temperature and millikelvin temperatures. The cold also makes springs slightly stiffer.

Prior to the improvements done to the mass-spring system as the cryostat was nonoperational, the masses had the springs attached to them on the outside of the masses (Figure 3.5). The purpose of this setup was stability in the rotational modes, along with an expected reduction in high-frequency resonance of the mass-spring system which could interfere with the SQUID data. However, it was uncertain whether a well-centered mass-spring system with springs attached only in the middle of each mass would be an improvement to the vibration isolation, or rather a downgrade.

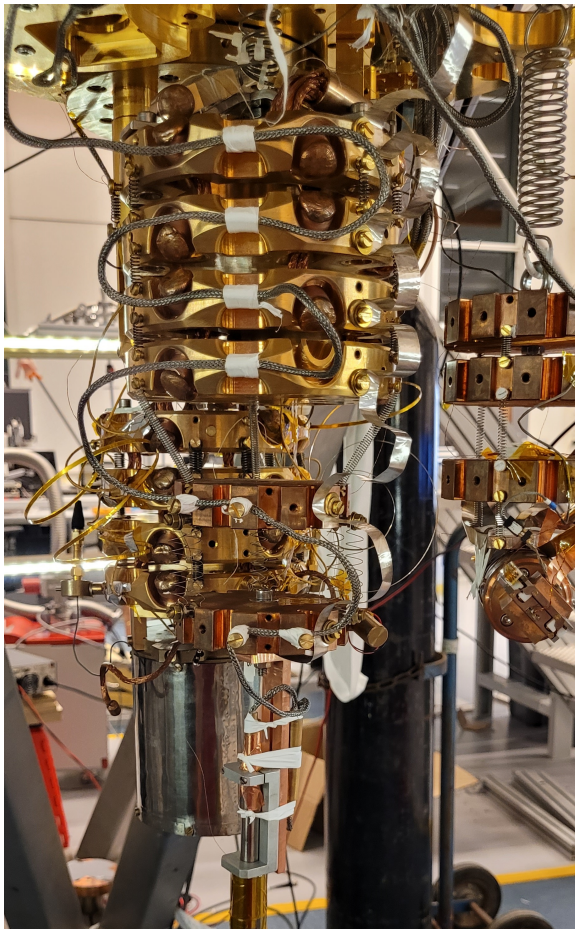

Figure 3.5: *Picture of the old mass-spring system, with the clamp attached to the lowest mass and springs at the sides of each mass.*

3.3.1 COMSOL simulation

To answer the question whether it would be a good idea to implement a center-suspended-only mass-spring system, we invoked COMSOL Multiphysics, a general physics simulation program. The goal of the simulation process was to determine which combination of springs and masses would result in the lowest eigenfrequencies and highest damping. More precisely, it was imperative to avoid eigenfrequencies of the mass-spring system from coinciding with the range of the mode frequencies of the Zeppelin, so that it would be certain that peaks in the spectrum between 15 Hz and 120 Hz would be true mode resonances.

Due to the masses already having been manufactured, with the hooks of each mass being very precisely in the middle of the mass, the springs were the only free variable left to vary. A COMSOL model was built (Figure 3.6), and a parametric sweep was taken with varying spring thicknesses, corresponding to different spring constants.

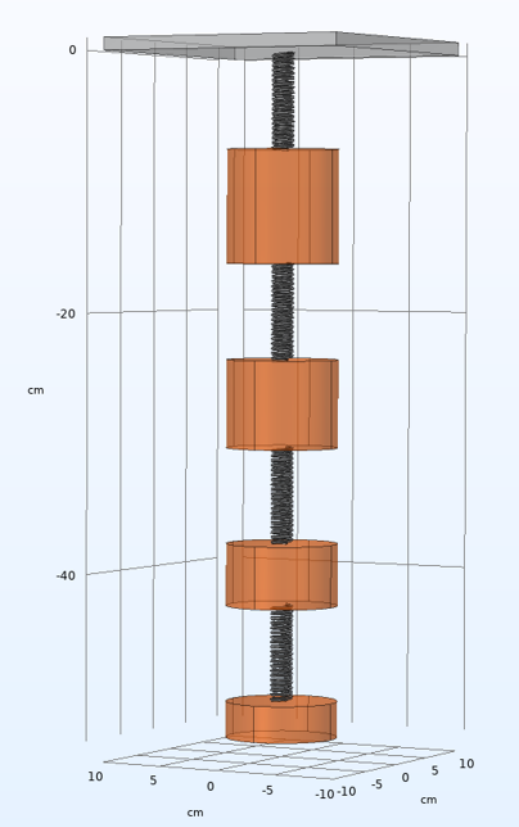

Figure 3.6: *COMSOL model of the new mass-spring system.*

For each combination of spring thickness parameters, COMSOL found 24 eigenfrequencies, corresponding to 6 degrees of freedom for every of the 4 masses (Figure 3.7). Higher eigenfrequencies could also be viewed, but these were clearly nonsensically high frequencies associated with the eigenfrequencies of just the springs themselves, which would be negligible in the SQUID measurements

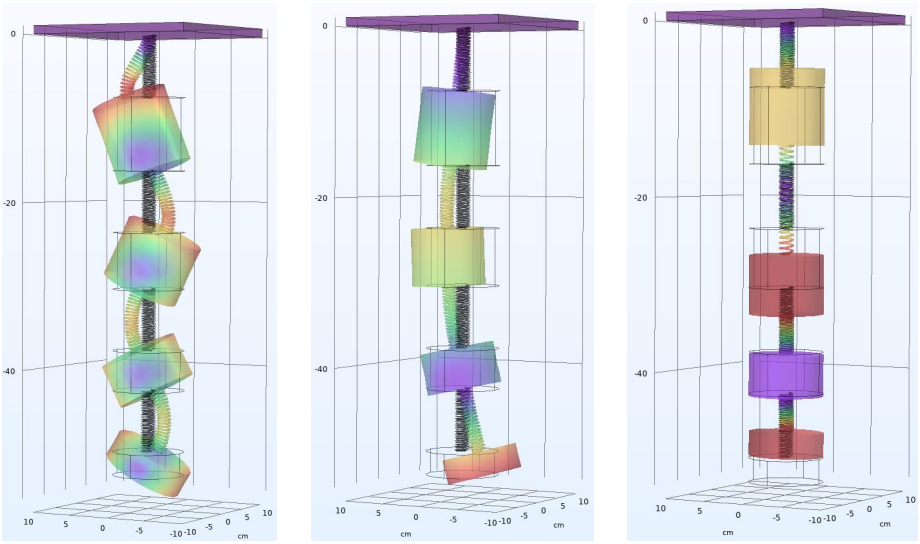

Figure 3.7: *3 of 24 eigenfrequencies as found by the COMSOL simulations.*

The parametric sweep returned an unexpected yet welcome result: no specific combination of spring thicknesses yielded an eigenfrequency higher than a combination which utilized higher spring thicknesses. In other words, it seemed that there was barely any resonance present between the different springs, implying that the way to obtain low eigenfrequencies was simply to acquire the most weak springs available, which would still be able to withstand the weight of the masses underneath them.

The COMSOL simulation did have a flaw: lack of gravity. While COMSOL did understand that the system was subject to gravity, as was visible from the time-dependent simulation, it did not adjust any eigenfrequencies in the presence of gravity. This is understandable for the pure spring modes, since the eigenfrequency of a spring is independent of gravity; however, modes which include a swinging motion should have been evaluated to have eigenfrequencies depending on the presence of gravity, which was not the case. Swinging motion having a low frequency, though,

it was decided to be best to interpret the results of the simulation as an invitation to acquire weak springs and substitute the old mass-spring system with a new, center-suspended-only mass-spring system.

3.3.2 Improved mass-spring system

Inspired by the result of the promising COMSOL simulation, springs were acquired and a new mass-spring system was built and suspended in the cryostat (Figure 3.8).

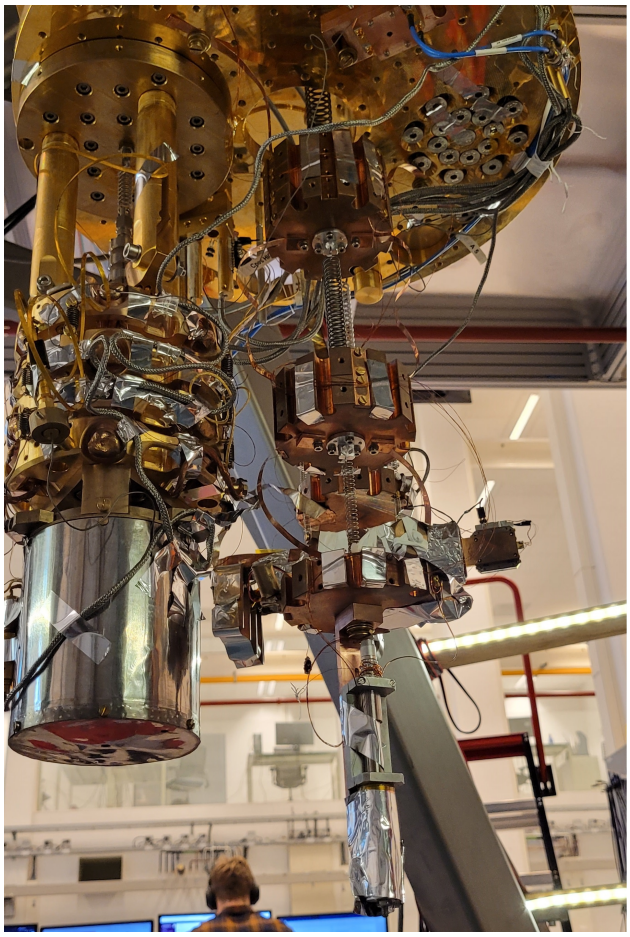

Figure 3.8: *Picture of the new mass-spring system suspended in the cryostat (right), with springs only between the centers of the masses. The top spring reaches up to the space between the 50-mK plate and the still plate.*

Three masses were ultimately used, weighing 2681 grams, 1835 grams, and 897 grams respectively in order from top to bottom, with a measurement error of approximately 2 grams. The three corresponding springs

have stretched lengths of 300 mm, 110 mm, and 70 mm, though these lengths are before contraction by millikelvin temperatures. The corresponding spring constants are 109 N m^{-1}, 480 N m^{-1}, and 210 N m^{-1}, corresponding to resonance frequencies of approximately 1 Hz, 2 Hz, and 2.2 Hz respectively. As the COMSOL simulation implied these frequencies would not interfere, this new mass-spring system is expected to be an excellent damping for vibrations in the z direction, its main restriction being the available height in the cryostat.

3.3.3 Lateral damping

Another improvement made to the vibration isolation was a block of lead (Figure 3.9) placed in the cryostat on leaf springs, designed to damp exceptionally in the x and y directions, seen as suspending all masses from their center is excellent for damping in the z direction, but leaves them susceptible to lateral vibrations.

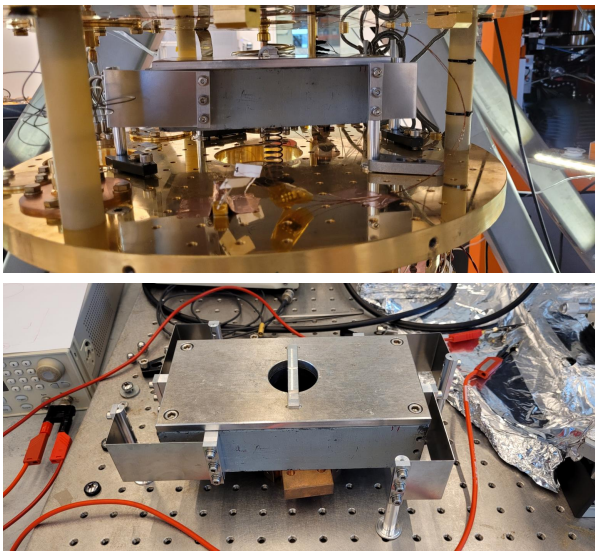

Figure 3.9: *Pictures of the laterally damping lead block. Top: fixed in the cryostat with the mass-spring system attached to it. Bottom: on a table with its leaf springs visible.*

This 11 kg block of lead was placed on the 50mK-plate, and from it the new mass-spring system was suspended through the hole in the block. The block itself was thermalized to the 50mK-plate. It was measured by video that the resonance frequency of the block was 2.3 Hz in the long

direction, and 2.5 Hz in the short direction, which is again sufficiently low that it should not interfere with the Zeppelin data. L-shaped leaf springs were chosen, as opposed to equally long springs in both axes, to separate the eigenfrequencies of the x and y directions. In combination with the exceptional improved mass-spring system, the laterally damping block of lead promises a new level of vibration isolation, taking another step in the direction of thermal limitation.

3.4 Moon simulations

Equation 2.18 provides an expression for the extremes of the changes in gravitational acceleration due to tidal forces, but the actual time-dependent course $g(t)$ is notoriously difficult to simulate precisely; the first paper to write out a comprehensive set of simulation equations (Longman, 1959)[4] starts its theory section by defining 50 parameters. Thankfully, a Python package called *tidegravity.py* based on this paper already existed for lunar and solar tide simulations. We adapted this package to be able to compare to the z mode frequency data of the Zeppelin by virtue of Equation 2.25. Understanding the *tidegravity.py* model constituted a significant part of the comparison process, as tidal forces are unintuitive, even for well-versed professors in Astronomy. Several test simulations were performed to inspect the behavior of the tidal forces (Figures 3.10, 3.11, 3.12).

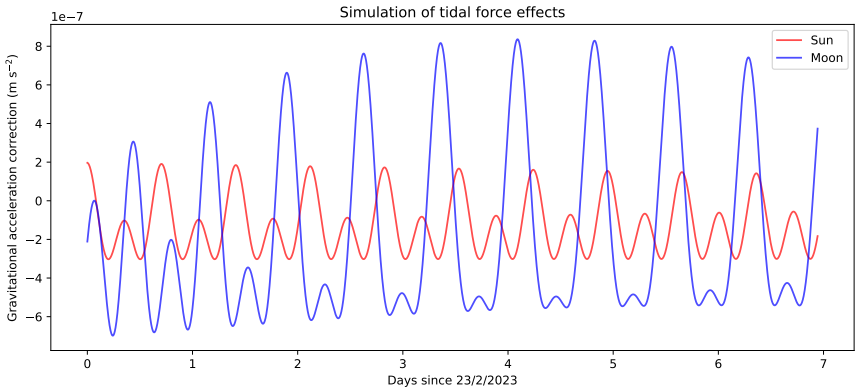

Figure 3.10: `tidegravity.py` *simulation of one week of the correction on* $g(t)$ *as a result of lunar gravity. The blue graph represents the lunar contributions, whereas the red graph represents solar contributions.*

Several observations can be made in Figure 3.10. Firstly, it shows that though the contribution of the Sun is less significant than that of the Moon, it is not entirely negligible. The graph also shows an unsurprising periodicity of the Sun of 24 hours, implying that the Sun returns to approximately the same location relative to the experiment every 24 hours. For the Moon, this periodicity seems to be 25 hours; the Moon's orbital period around the Earth being 27 days, in the same direction as the Earth rotates, it expectedly takes the Moon slightly longer to return to the same location in the sky.

Both Sun and Moon show roughly two peaks and two troughs every period. This effect is expected, as the tidal forces pull upwards twice a day: once with the celestial object directly overhead, and once directly beneath us, which can be made intuitive by viewing it as the object pulling the Earth away from us (Figure 2.4), effectively decreasing the gravitational force. This double frequency is common knowledge in context of ocean tides. Contrary to ocean tides, though, the effect of the higher peak tide during a period can be many factors larger than the lower peak. Ocean tides experience other effects, such as fluid dynamic resonance, due to which the relationship between their height and the local tidal forces is more complicated.

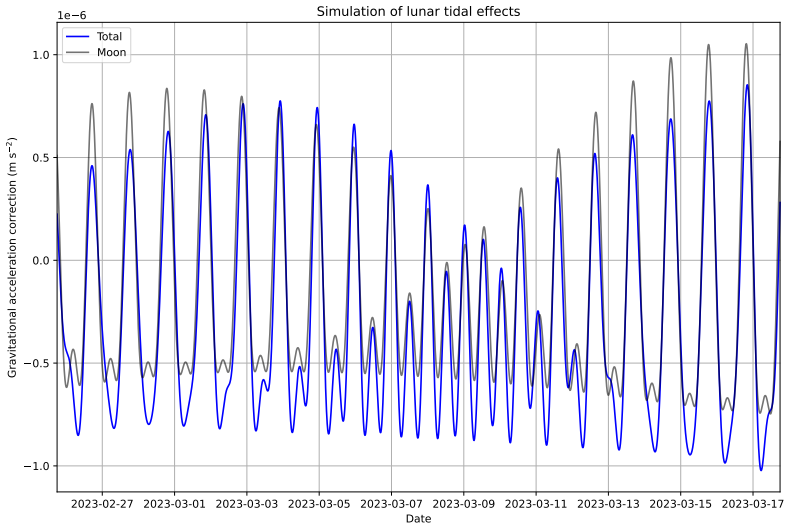

Figure 3.11: *`tidegravity.py` simulation of 20 days of the correction on $g(t)$ as a result of lunar gravity. The blue graph represents the sum of solar and lunar contributions.*

The ratio between this higher and lower peak also changes significantly over time, especially in the case of the Moon. Figure 3.11 shows this more clearly: it seems that the highest peak of each period itself is contained in an envelope with a period of one lunar month, or 27 days. Intuitively, this makes sense: after half a lunar month, the Moon is on the other side of the Earth at the same time of day, thereby inverting the roles of the higher and lower peaks of each period. Because this inversion process is gradual, the higher and lower peaks occasionally coincide, as seen in the middle of Figure 3.11. A more rigorous explanation is as follows: as seen from the experimental frame of reference, the position of the Moon experiences a 25-hourly periodicity as a result of its 25-hourly reappearance at the same azimuth, physically corresponding to the Earth having rotated around its axis. Furthermore, the position of the Moon experiences a 27-daily periodicity as a result of its 27-daily reappearance at the same altitude, corresponding to the Moon having completed an orbit around the Earth. This second periodicity arises from the lunar orbit being inclined by some 30° with respect to the rotational axis of the Earth. A multiplication of the two periodic motions yields a 25-hourly periodic graph within a 27-daily periodic envelope, as seen in Figure 3.11. For the Sun, the envelope period should be expected to be a solar year, i.e. 365.24 days.

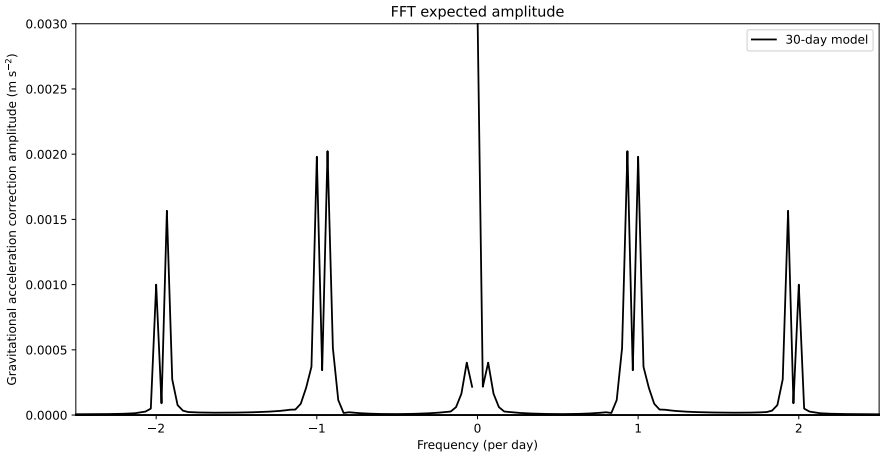

Figure 3.12: *Fast Fourier Transform amplitude plot of* `tidegravity.py` *simulation of 30 days of the correction on $g(t)$ as a result of lunar gravity. 30 days of model time were necessary for distinguishability between the 24-hour and 26-hour peaks.*

Figure 3.12 shows the amplitude of a Fast Fourier Transform (FFT) of a 30-day model of lunar gravitational acceleration correction data. Taking an FFT is a crucial step in the comparison between the Zeppelin frequency data and the model, as it separates the 24-hour periodicity associated with most of the daily processes potentially influencing the Zeppelin from the 25-hour periodicity of the Moon. The expected Fourier spectrum of a 25-hour periodic signal enveloped in a 27-day periodic signal, which is a multiplication of two periodic functions, should approximate a peak at a frequency of 1 per 25 hours convolved by a peak at a frequency of 1 per 27 days, resulting in peaks around the 24-hour and 26-hour marks. As the graph shows, 30 days is a sufficiently long integration time to split the 24-hour peak, the rightmost of the two peaks at the *1 per day* mark, from the 26-hour peak, the leftmost of the two. The fact that there is a 24-hour peak in the FFT of the model is correct, albeit unintuitive: the 24-hour cycle of the Earth is, after all, the true physical process represented by a 24-hour peak, whereas the 26-hour peak is essentially an artefact caused by convolving the 25-hour peak with the extra daily hour of the 27-day physical process which is the orbit of the Moon around the Earth. The 26-hour peak, however, is more important for comparison of Zeppelin data, as a measured 24-hour signal could be attributed to many processes, whereas the 26-hour peak of the Moon is comparatively unique.

Chapter 4

Results

When the cryostat is nonoperational, much effort can be made to benefit the experiment: improving vibration isolation, improving the Zeppelin, modeling, and innovating; but once the cryostat is operational and sufficiently cold, the SQUID provides a constant time-varying signal, and it is only a matter of registering the signal, sometimes manipulating it by exciting the Zeppelin by engaging the piezo element, and performing an analysis on the results to quantify the modes in various ways.

The results section aims to do exactly this: present the SQUID data in different ways and contexts, so that it may be used as a milestone to compare with in the future. After all, the quest to obtain a hypersensitive quantum-scale gravity sensor is tedious, and the results of this experiment are a small but significant step in that direction; even though we are a long way away from quantum gravity, we still work with state-of-the-art equipment and data analysis, producing results which push the boundaries of the many skills necessary to arrive there eventually. Therefore, the results do not work towards any single value, but rather broadly describe the current state of the system we use to detect changes in gravity.

The results are split into different sections consisting of the SQUID data spectrum, an quantitative overview of the modes, the stability of their oscillation frequencies, an observed coupling effect between modes, force noise measurements, and finally, whether the Moon was detected.

4.1 Spectrum

The most straightforward method to analyse SQUID data is to directly take its spectrum. The read-out program of the SQUID automatically performs a spectrum analysis, as seen in Figure 4.1.

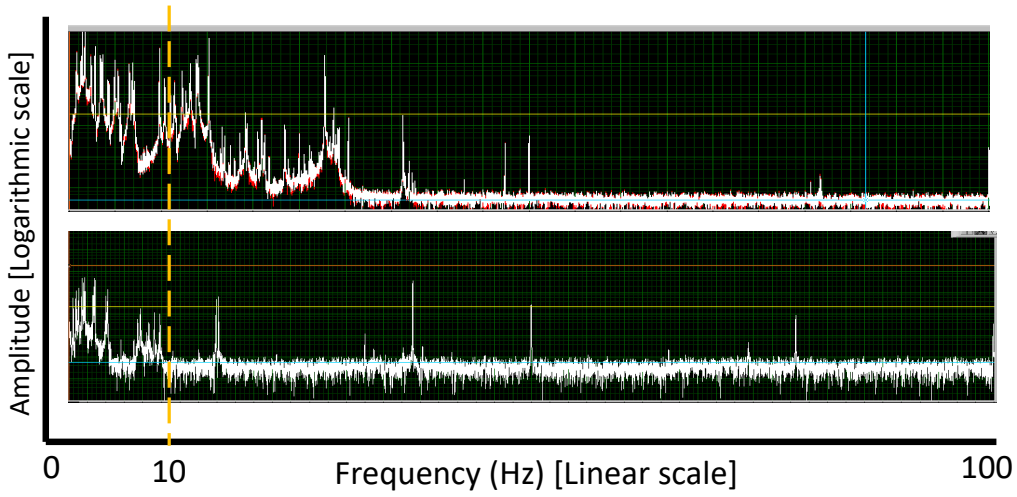

Figure 4.1: *Spectra generated directly from SQUID data from the Zeppelin, where 0 Hz and 100 Hz indicate the start and end of the spectral regimes. The top spectrum is from before adjustments to the mass-spring system; the bottom spectrum is after adjustments. It is evident that the improved vibration isolation damped significantly more noise, especially at frequencies greater than 10 Hz, as all its intrinsic resonances lay at lower frequencies.*

Figure 4.1 shows that the implementation of the new vibration isolation with the laterally damping block of lead and the centrally suspended mass-spring system makes a world of difference in the spectrum. The top graph noise, presumably intrinsic vibrations of the old mass-spring system, extends all the way into the 30 Hz range, which is already in the range of the first modes. Meanwhile, the bottom graph shows that the noise is acceptably flat already from 10 Hz, which is before the lowest-frequency mode.

It is greatly desirable that the lowest modes not overlap in frequency with the intrinsic noise, as overlapping can mean that the mode in question is unintentionally being stimulated by the mass-spring system vibrations. Overlap can also lead to misleading values after performing lock-in analysis, i.e. integrating the spectrum locally near the frequency of the

modes, to determine the energy in a given mode. Integrating a mode which overlaps with noise would give it a higher energy value, making it more difficult to directly compare with other modes which have less noise. Whereas the absence of high-frequency noise does not directly imply an improved mode quality as such, it is an excellent indicator of the improvements that the new vibration isolation introduced.

4.2 Overview of modes

Quickly summarizing, the Zeppelin has six modes in total: three rotational and three vibrational modes, corresponding to the three rotational and thee vibrational degrees of freedom of a free, rotationally asymmetrical rigid object. By *mode* we mean an oscillation at a specific frequency in one of these degrees of freedom.

Which frequencies the Zeppelin exactly oscillates at is in itself not of utmost importance. The frequencies tend to change each time the Zeppelin falls to the bottom of the trap and starts levitating again, which usually only happens either as the cryostat is being opened, or due to malfunctions. The changes in frequency due to such a drop-and-levitate can amount tens of percent. On a weekly scale, modes also tend to show a linear frequency shift which is often of higher order than the variations within a day, possibly due to flux creep. However, it is possible to determine the approximate mode frequencies mathematically, as seen for the z and β modes in Equations 2.10 and 2.11. Back-of-the-envelope calculations for the other four modes have shown that the x and y vibrational modes are most likely the two lowest-frequency modes, whereas the z mode could be either the third or the fourth. The remaining α, β, and γ rotational modes then occupy the other three frequencies.

It should be noted that the spectrum does not explicitly distinguish between modes. While magnetic excitation does allow us to confirm whether there is a mode at a given frequency, which is how the six modes are found in the first place, giving each mode a physical interpretation does to some extent stay a matter of speculation.

Though it is not possible to reproduce specific frequencies consistently, and though it is not possible to be certain of the physical interpretations of each mode, it is possible to consistently find all six modes in the same frequency range: between 10 Hz and 150 Hz. As an example, the most recent list of mode frequencies was: 15.0 Hz, 15.6 Hz, 31.9 Hz, 36.7 Hz, 71.6 Hz, and 77.0 Hz.

To start truly quantifying the performance of the modes, we reintro-

duce Equations 2.14 and 2.15. The goal is to obtain a high quality factor (Q) across all modes, while simultaneously keeping the mode temperature T_{mode} as low as possible. Ideally, all modes would have a corresponding temperature $T_{\text{mode}} = T$ where T is the temperature of the surroundings, which in case of perfect thermalization would be the temperature of the mixing chamber plate, approximately 10 mK in the best case. As T_{mode} approaches T, we speak of the system becoming thermally limited. However, it is still imperative that low mode temperatures not be a result of a low quality factor, as this would be counterproductive.

4.2.1 Quality factor

The quality factor Q expresses the number of individual vibrations a mode takes to diminish in amplitude by a factor e^{-1} after being excited to a higher energy, for example by the piezo element. Performing this calculation for the Zeppelin under the old and and new mass-spring systems yielded Figure 4.2.

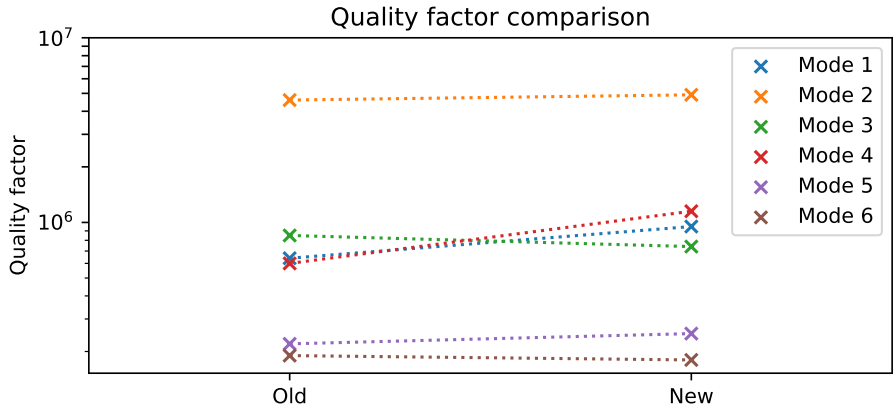

Figure 4.2: *Change in the Zeppelin's quality factors between the old and new mass-spring system for all six modes.*

Figure 4.2 shows that the quality factors of the modes did not necessarily improve as a result of the new mass-spring system, but stayed at impressive levels, one of them even reaching 4 million.

4.2.2 Mode temperature

Similarly, the mode temperature T_{mode} expresses an effective temperature characterizing the amount of energy in a mode, therefore measured with-

out excitation. The energy in the harmonic oscillation is expressed as a temperature by dividing by k_B, the Boltzmann constant, which relates energy to temperature. Performing this calculation for the Zeppelin under the old and and new mass-spring systems yielded Figure 4.3.

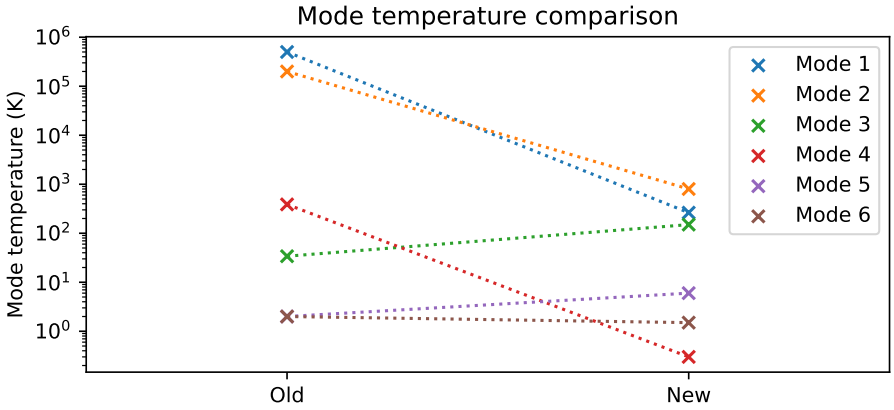

Figure 4.3: *Change in the Zeppelin's mode temperatures between the old and new mass-spring system for all six modes. Blue and orange correspond to x and y modes.*

Figure 4.3 shows that the temperatures of the modes are generally lower after the upgrade of the vibration isolation. Especially the two lowest modes showed a significant improvement, possibly as a direct consequence of the implementation of the laterally damping block of lead causing less excitation. Together with the result of the quality factors, however, this result is more impactful, as it implies that the temperatures of the modes managed to be subdued without harming the quality factor.

4.3 Frequency stability

Frequency stability is another, more long-term measure for the quality of the modes. Ideally, a given mode which is not being excited stays at a fixed frequency forever, only being influenced by changes in gravitational acceleration if the mode in question has gravity as a restoring force, such as those due to the Moon. However, in practice, the frequency of modes tends to drift linearly, or, more frustratingly, vary at random, especially during daytime. We have had various hypotheses about the origin of the frequency variations: variations in air pressure, electric network noise, nearby traffic, etc.

When there is a period of relative stability, often at night, the stability can be quantified in terms of the phase variance. The phase is directly linked to the frequency: if a mode's phase stays precisely constant during a given time frame, then so will its corresponding frequency. Using the Zeppelin's phase data from the lock-in amplifier, we can determine the variance in the phase and the time in which the variance took place, and translate to a maximum variance in frequency (Figure 4.4).

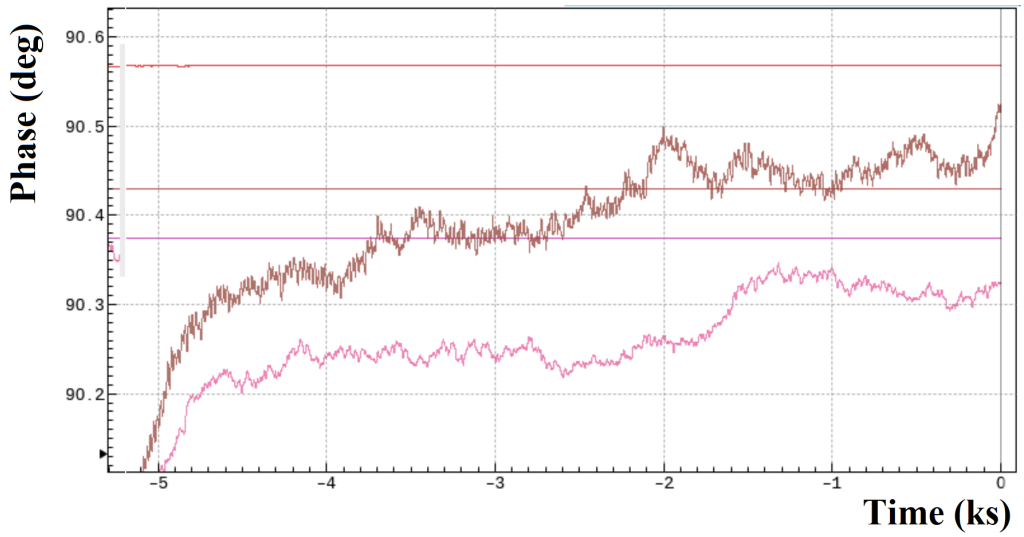

Figure 4.4: *Phase plots of mode 5 (brown, 71.6 Hz) and mode 6 (pink, 77.0 Hz). Between -4 ks and -3 ks, mode 6 shows a phase variance of no more than 0.03 degrees, or 108".*

Figure 4.4 is most interesting in the 1000 seconds between the -4 ks and the -3 ks mark. In this time, the variance in phase of the pink 77 Hz mode is no more than 108". This implies a maximum frequency drift of $108''/2\pi$ per 1000 seconds, which amounts to $8.3 \cdot 10^{-8}$ Hz. As this mode operates at 77 Hz, the relative drift during this time, calculated by dividing the maximum frequency drift by the mode frequency, is $1.08 \cdot 10^{-9}$, approximately one part per billion. This is a stunning result, implying that at times, we can know the oscillation frequency of one of the modes of our Zeppelin at nine significant digits of precision. Naturally, this was an exceptional measurement; usually, the phase was only stable enough to measure frequencies at slightly lower precision.

4.4 Mode coupling

Mode coupling, in its most general description, is the phenomenon that the properties of one mode are dependent on the energy in other modes. Quantifying this coupling of modes is crucial because it demonstrates our ability to control the energy levels of the modes to some extent, seen as we are capable of simultaneously reading out and exciting all the modes. By adjusting the excitement amplitude of a mode, we can consistently observe the consequences for the other modes. Considering the ultimate goal of making all modes vibration-free, an optimization process can be envisaged where the six modes are controlled in a way that minimizes the total energy. The more data we generate on the couplings between the modes, the more feasible it becomes to carry out such an optimization process.

A simple way to quantify mode coupling is to drive one mode at a certain amplitude, to drive a second second mode to some beginning amplitude, and subsequently determine the decay time of the second mode, repeating the measurement for different amplitudes of the first mode (Figures 4.5 and 4.6).

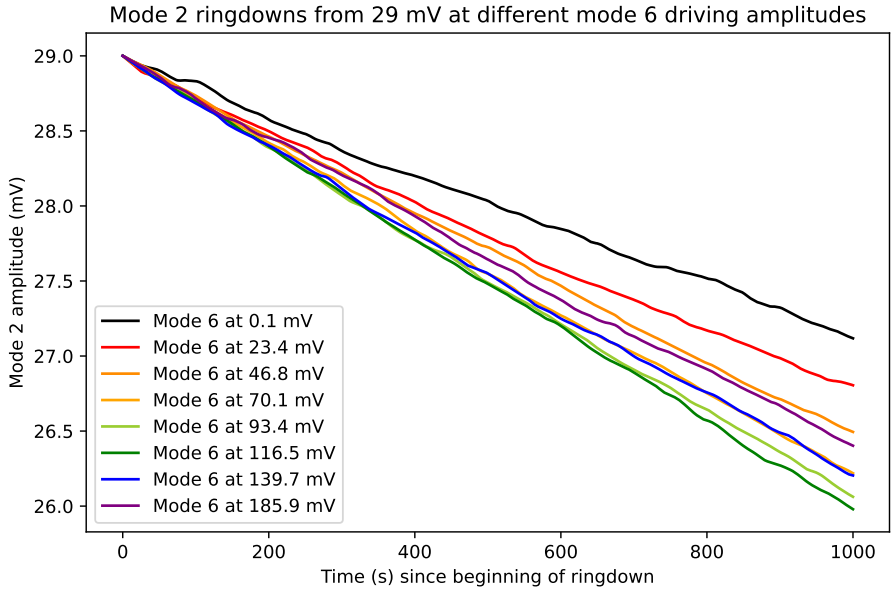

Figure 4.5: *Decay plot of mode 2 at varied mode 6 driving amplitudes. Mode 2 starts it decay at 29mV.*

Such a process was done twice, both times between modes 2 (second-to-lowest frequency mode) and 6 (highest frequency mode). Mode 6 served as the constant driving amplitude, of which the amplitude was varied for each decay measurement, whereas mode 2 served as the decaying mode, which started at a fixed amplitude. This amplitude was chosen 29 mV for the first measurement, inducing comparatively short decay times (Figure 4.5), and 9.9mV for the second measurement with longer decay times (Figure 4.6).

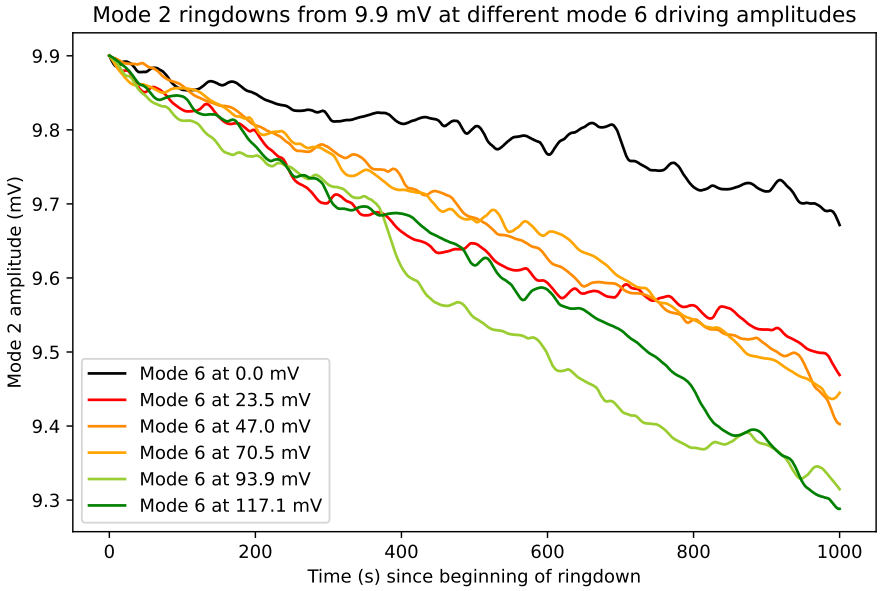

Figure 4.6: *Decay plot of mode 2 at varied mode 6 driving amplitudes. Mode 2 starts it decay at 9.9mV.*

These measurements can be combined into a single figure (Figure 4.7), where the coupling is now given in terms of energy and corresponding quality factors. The figure, especially the high-energetic decay, shows that there is a value of mode 6, approximately 1500 eV, for which the quality factor of mode 2 is lowest. The non-monotonic behavior should come as a surprise, as there is no apparent reason for the quality factor to start rising with mode 6 energy. The data points of the low-energy decays are too noisy to make a conclusive statement.

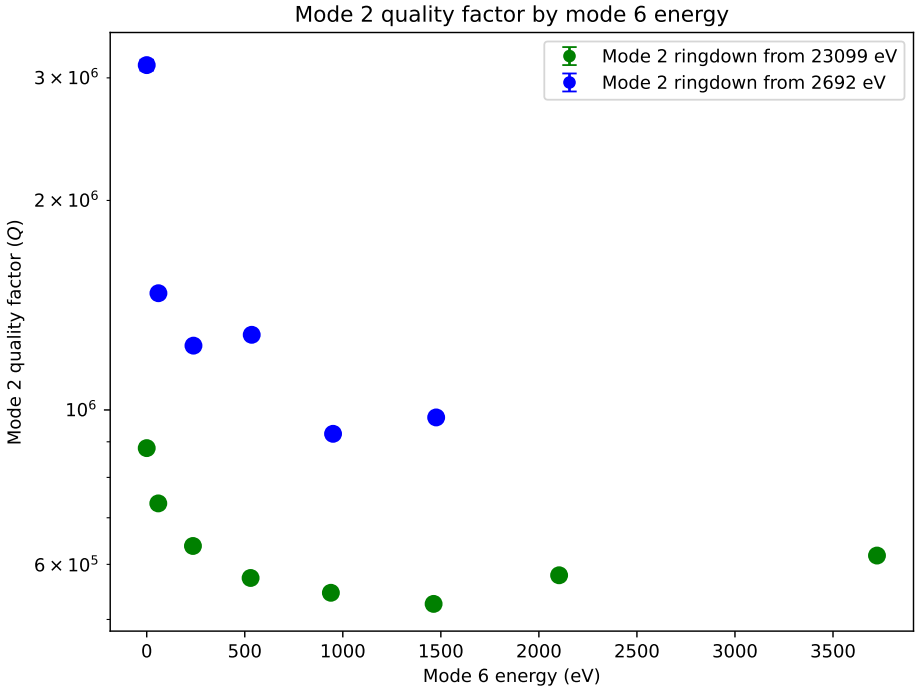

Figure 4.7: *Combined plot displaying the dependence of the quality factor of mode 2 on the energy in mode 6, as translated from its amplitude. Q was calculated using decay times found from Figures 4.5 and 4.6.*

Figure 4.8 provides a self-consistency measurement, showing that the decays barely contain a random component, by performing multiple decays at the same mode 6 driving amplitude. The variation in the decay times is approximately 1%, which implies that mode coupling is the real cause of the effects seen in Figure 4.7, rather than random variations in the decay time caused by external factors.

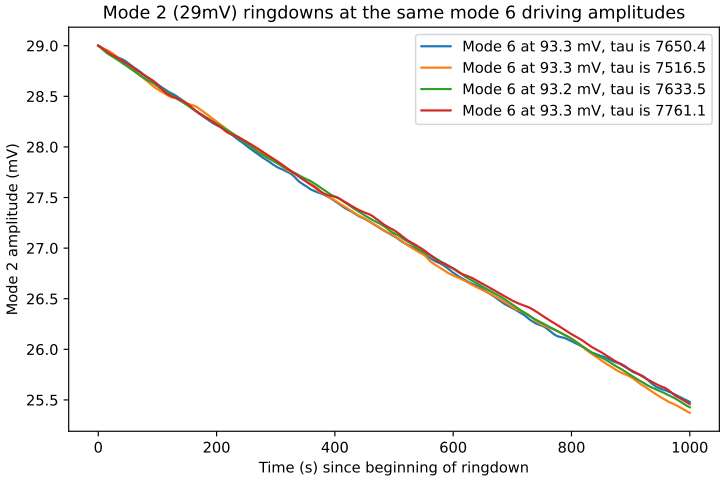

Figure 4.8: *Self-consistency plot showing the decays of mode 2 under the same mode 6 driving amplitude, with variations in decay time not exceeding 1%.*

4.5 Force noise

While quality factor and mode temperature measurements are excellent indications of mode performance, force noise is the most scientific of the three (Figure 4.9).

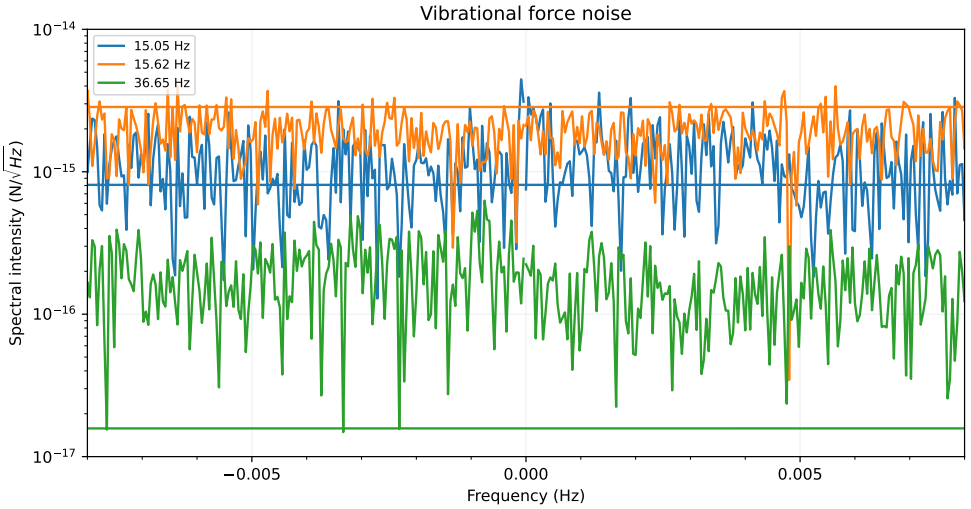

Figure 4.9: *Force noise of the three suspected vibrational frequencies. Rotational frequencies were omitted, as there was uncertainty with regards to the dimensional analysis.*

As is often the case with scientific methods, the first step in calculating force noise is taking a Fourier Transform. For force noise, the amplitude of a specific mode as a function of time, as determined by a lock-in amplifier, is converted by FFT to a frequency-dependent amplitude. This result is then compared to the transfer function of a driven harmonic oscillator with the same frequency range (Figure 4.10). The former is divided by the latter to obtain the force noise, as seen in Figure 4.9.

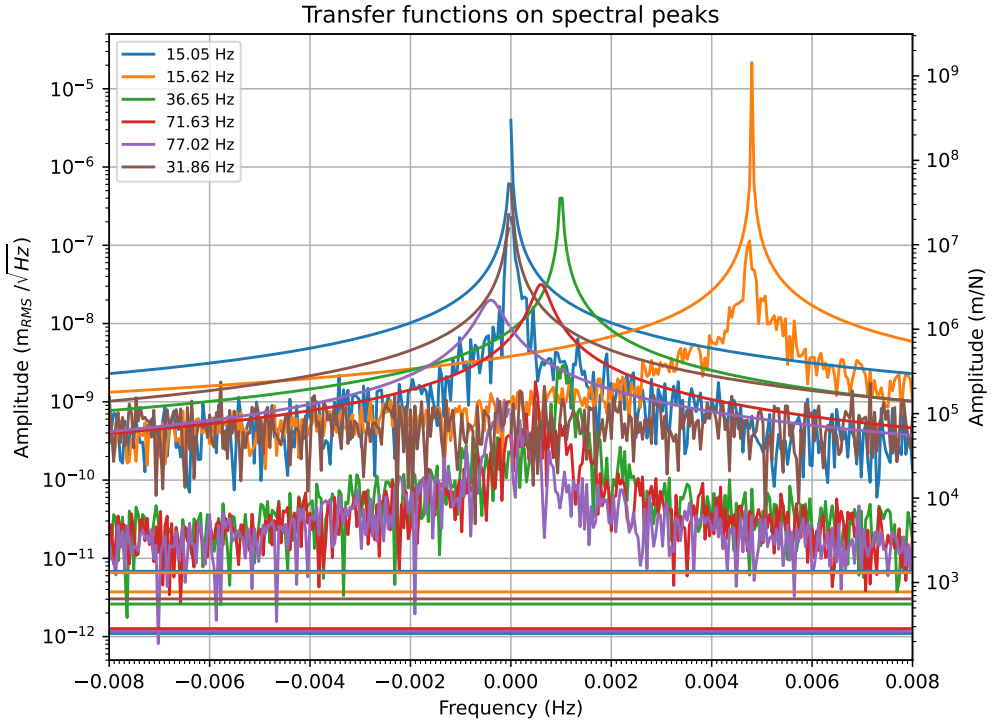

Figure 4.10: *FFT of all six modes of the Zeppelin with overlaying transfer functions, relative to their resonance frequency. The force noise can be used to more precisely calculate the mode temperatures using the equipartition theorem.*

4.6 The Moon

The crux of the experiment was, of course, to be able to see the Moon in the measurements. Disappointingly, however, at the time of the data analysis, the system was simply not sensitive and noise-free enough to see the Moon (Figure 4.11). A lot of time was spent improving the setup and quantifying the new SQUID data, leaving no time for a lunar retake. Alas, all good things must come to an end, and so do the results of this thesis, with no Moon in sight.

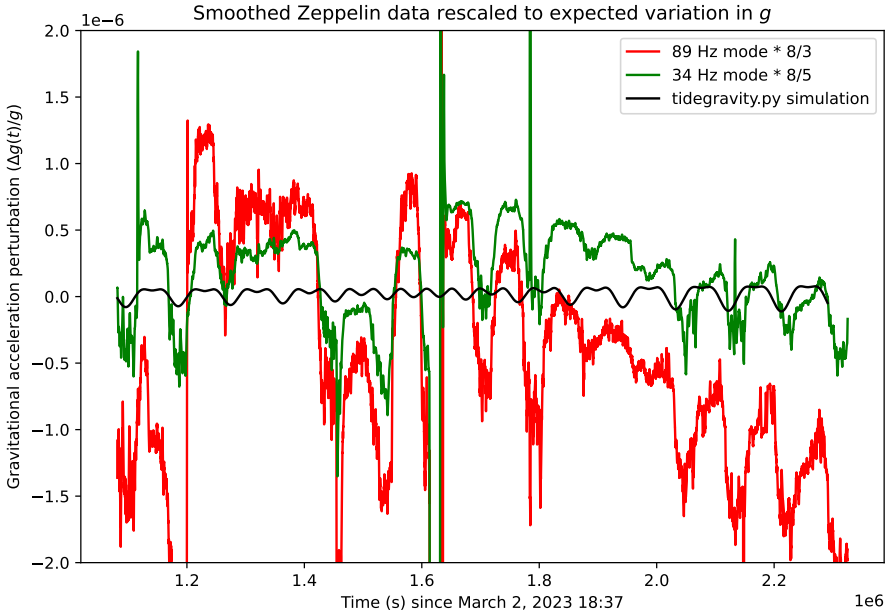

Figure 4.11: *Plot showing a set of relatively stable data in the suspected z mode (34 Hz) and β mode (89 Hz), normalized as described in Equations 2.25 and 2.26, in combination with the expected lunar effect on the relative gravitational acceleration, which is too small to see. An FFT of 30 days of (partially extrapolated) frequency data yielded equally unsatisfactory results.*

Chapter 5

Discussion

Most interpreting of the models and specific results was already done in their respective sections, but the discussion section introduces a more general overview of which issues arose while performing the experiments or data analysis. We consider a variety of topics: why tides should be the dominant perturbation of gravity, what further improvements can be made to the setup, in which way the SQUID data could be analyzed more rigorously, whether some data could be corrupted due to incorrect dimensional analysis, and finally, whether the Moon could become visible in the near future.

5.1 Tidal domination

As is evident from Equation 2.18, the effect of tidal forces on gravitational acceleration is a higher-order effect than direct gravity, as it is a gradient, which is why it only contributes to variations in g seven orders of magnitude smaller than g itself. However, calculating the direct effect of the gravitational pull of the Moon by Newtonian gravity, which is hence of the same mathematical order as Earth's gravity, yields an amplitude of $4 \cdot 10^{-6} g$. For the Sun, this effect is as large as $6 \cdot 10^{-4} g$. Unsurprisingly, the direct effects are much larger than the tidal effects, which are of the order $10^{-7} g$; and yet, in each model of the time-dependent and location-dependent gravitational acceleration, tidal effects are taken to dominate, while direct effects are neglected. The same goes for gravity measurements performed by highly sensitive gravimeters.

This seeming discrepancy was often a topic of confusion, even leading us to invoke the aid of professors from the Leiden Observatory, to no

avail. Ultimately, though, we did come up with a possible explanation. The direct gravitational pull of other celestial bodies than the Earth pulls the Earth everywhere with an equal acceleration in first order. Each object on Earth is accelerated towards the body at the same pace, including both the Zeppelin and the entire measurement system. Therefore, in the Earth's frame of reference, this does not cause a change of perceived gravitational acceleration in first order. However, in second order, as the Earth is deformed due to the differential of gravitational acceleration, the distance between the Zeppelin and the center of mass of the Earth does change; and since the measurement setup is connected to the Earth, whereas the Zeppelin is not, the second order effect is in fact directly measurable, leading it to dominate the variations in g.

5.2 Setup improvements

The current experimental setup is in essence quite simple, so many components can be added to improve its various aspects. One immediately obvious improvement would be to add more mass and longer, weaker springs in the mass-spring system, which would inevitably improve the damping. The main limiting factor for this improvement is the size of the cryostat. Another way to obtain vibration isolation is by using an inverted pendulum system or a string-suspended mass-spring system, though such measures introduce many complications. A comparatively low-effort change to the Zeppelin would be to use magnets coated with non-magnetic material, removing the threads mentioned in the methods, and thereby decreasing magnetic damping and possibly limiting non-linearities. Adding more piezo elements, to improve the control of the mode excitations, is another logical improvement.

The more challenging improvements are those which limit the induced vibrations prior to them entering the cryostat. Tilting the frame of the cryostat, by putting heavy bags of lead on one of the legs, was measured to have drastic effects on the frequencies of the modes, signaling the importance of a well-leveled cryostat. Improving the active feedback on the block of concrete on which the cryostat frame stands is therefore a key factor.

The suspected main cause of induced vibrations is the pulse tube (PT) which practically shakes the cryostat every 0.7 seconds. Since this vibration is highly constant over time, it would be appropriate to use a Kalman filter to cancel some of the vibrations actively, without feedback. Currently, we occasionally use PID feedback to control the frequency of the

modes instead, but the tuning and running is done by hand; automation of this process would be a possible alternative to introducing a Kalman filter.

Some more ambitious ideas have also been proposed over the course of the experiment, a main one being the Leiden Cryogenic Drop Tower (LCDT): a cryostat placed above a cylindrical hole in the ground which would be tens of meters deep, allowing experiments to take place in cryogenic temperatures, pressures and free-fall, allowing for yet more accurate measurements.

5.3 Analysis improvements

As the amount of data produced by the SQUID is on the order of gigabytes every day, which is enormous, there are many possibilities for extracting more qualitative data or improving the data. Any operation on data can only reduce the total amount of information, but with the amount of available data, this is not a factor.

In the current analysis of the frequency of each mode of the Zeppelin as provided by the lock-in amplifier through which the SQUID data passes, the given frequency is taken for granted. However, this frequency can deviate from the true oscillation frequency of the Zeppelin through numerous artefacts. Most notably, the time-derivative of the phase directly results in an equally large frequency shift. The amplitude changing in time also influences the phase, which in turn changes the frequency. Finally, the angular difference in phase between the true phase and the excitation phase causes a quality factor-dependent frequency shift. Understanding and being able to account for all these effects automatically could improve the frequency data to a higher accuracy, especially once vibrational noise is sufficiently diminished.

Moreover, many steps in the current analysis methods are done by eye. This is unavoidable in experimental physics, especially in systems where all factors influence each other and there is no way to get a truly independent measurement. However, determining the position of the transfer function peak in Figure 4.10, the variance in phase in Figure 4.4, or the random motion as needed to calculate the mode temperatures in Figure 4.3, was all done by eye. Automating these processes is a way for future measurements to be more accurate and reliable.

5.4 Dimensional analysis

In much of the data analysis performed, all six modes are treated equally. For instance, in Figure 4.10, all modes are plotted with units of m $\mathrm{Hz}^{-1/2}$ on the ordinate axis. It is possible to treat all modes as vibrational modes, but it is not entirely physical. Finding the rotational modes and labeling their properties accordingly would be more appropriate. This would mean, for instance, using $[\kappa] = \mathrm{N\,m\,rad}^{-1}$ as an angular spring constant, rather than the vibrational $[k] = \mathrm{N\,m}^{-1}$, which is now only done for modes 5 and 6. Similarly, the sensitivity of all modes is expressed in $\mathrm{V\,m}^{-1}$, whereas rotational sensitivity would be more physical if expressed in $\mathrm{V\,rad}^{-1}$.

The challenge in performing correct dimensional analysis is being able to separate the vibrational modes from the rotational ones with certainty, preferably based on another technique than only theoretical frequency comparison, as mode frequencies tend to differ drastically from their theoretical counterparts. As of yet, such a technique is not applied. One idea is to use an oscillating gravitational mass to induce gravitational attraction at the mode frequencies from outside of the cryostat in different directions, and combine the data to infer the direction of each mode. Another option is to improve the read-out: introducing a second SQUID, for example, would already make dimensional analysis a lot easier thanks to the newly introduced degree of freedom.

5.5 The Moon

The discussion of improvements reintroduces the question whether the Moon would be visible after these improvements. Figure 4.4 does indeed show that periods of extreme mode stability are possible, though Figure 4.11 shows that such periods of stability never last for weeks, which would be necessary to convincingly see the effect of the Moon. However, even during periods of extreme stability where the frequency variance was low enough to possibly see tidal influence, no hint of the Moon could be seen, let alone conclusive evidence. As the Moon definitely does exert gravitational influence on the Zeppelin, though, the only possible conclusion is that the signal-to-noise ratio must improve before the Moon can be distinguished from the nosie.

Since the long-term goal of the Zeppelin is to become an effective gravity sensor, a serious consideration to be able to test whether the Moon can

be seen under improved vibration isolation should be to invest in an extremely sensitive gravimeter, capable of sensing variations in g of $10^{-8}g$ or smaller. The data from a gravimeter next to the Zeppelin data would serve as a much more reliable control than the *tidegravity.py* simulations; not because the simulations were incorrect as such, but because the Zeppelin ultimately cannot distinguish between tidal gravity and other sources of gravitational acceleration variation, which we may have forgotten to consider. Gravimeter measurements could also serve as highly reliable control measurements for when gravity is artificially generated to test the Zeppelin's responsivity, potentially solving otherwise complex problems.

In the end, while it is definitely a pity that the Moon was not visible in our measurements despite her frequently watching over us from above, there is no reason why we should cease to improve our setup and analysis methods, possibly assisted by a gravimeter, as each step towards measuring the Moon is a step forward, in the direction of an extremely sensitive gravitational force sensor at microscopic scale.

Chapter 6

Conclusion

This experiment investigated the sensitivity of a small magnet called the Zeppelin, which was levitated by Meissner levitation in a tantalum well-shaped trap, which was superconductive due to the placement of the experiment in a cryostat. The three rotational and three vibrational modes, corresponding to the six degrees of freedom of the Zeppelin, were observed by a SQUID, and subsequently quantified into quality factors, mode temperatures, and frequency stability, as well as translated via a lock-in amplifier to a time-dependent frequency of each mode.

Since the gravitational acceleration on Earth depends on tidal forces of the Moon and the oscillation frequency of several modes depends on the gravitational acceleration, data analysis was performed on the aforementioned time-dependent frequency along with a model of the tides of the Moon and Sun, in hopes of being able to detect lunar patterns in the Zeppelin data. Unfortunately, the Zeppelin was still too noisy, especially at timescales of lunar periods, to conclude the presence of the Moon.

As the cryostat opened, efforts were made to improve the vibration isolation, including the installation of a laterally damping block of lead and a new mass-spring system, with the masses only attached to the springs at their center, aided by a COMSOL simulation. The new vibration isolation significantly improved the mode spectrum, the mode temperatures, and the frequency stability, which peaked at an impressive one part per billion. The mode coupling and force noise were also quantified.

With the improvements to the setup achieved during this experiment, combined with novel ideas for improvements to the setup and data analysis methods, there are bright prospects for the future of quantum-scale ultrasensitive gravitational force sensors; and one day, maybe, we may see the Moon.

Acknowledgements

To by dopiero jakiś chłopczyk uwielbiał, specjalne miejsce gdzie może sobię pisać co chce. Oczywiście, dużo rzeczy doprowadziło do tego, że ta praca została napisana i przy tym studia licencjackie zakończone, ale jednak w końcu to jedna osoba, zawsze radząc że mam się skupić na studiach, mnie wspierała jak nikt inny. Większość ludzi w moim życiu mi pomogła w jakimś sposobie, ale jedna osoba była nieporównywalnie niezbędna i to dlatego jej należy pierwsze miejsce w podziękowaniu. Mam nadzieję, że ta osoba siebie rozpoznaje w tym opisie—znając ją, wierzę, iż tak.

Naast alle vaardigheden die ik heb opgedaan tijdens dit onderzoek, heb ik vooral geleerd om op een geïnspireerde en creatieve manier het onderzoek te benaderen – iets wat zeldzaam is in de Natuurkunde, maar voor mij van ongeëvenaard belang. Dit was voor mij de pracht van het werken in de groep Oosterkamp. Ik ben Tjerk dan ook zeer dankbaar voor deze mogelijkheid.

Ik ben Tjerk en Dennis dankbaar voor hun waardevolle en geduldige begeleiding. Ik kan me voorstellen dat het niet meevalt om voor de elfde keer aan een bachelorstudent uit te leggen wat het verschil is tussen de SQUID en de lock-in. Ik zal met een warm hart terugdenken aan de momenten wanneer wij met zijn drieën de vreugde voelden van een platter spectrum of een negende decimaal.

Martijn, Reinier en Timo – mijn drie medebachelorstudenten in de groep Oosterkamp – hebben de eindeloze dagen in de Nieuwe Meethal niet alleen verdragelijk gemaakt, maar hebben het zelfs voor elkaar gekregen om mij ernaar te doen uitkijken. Al het fruit dat wij hebben gestolen, alle koffiemomentjes (of choco-crème-wienermelangemomentjes) die we hebben gedeeld, alle herinneringen die we hebben opgedaan in de Eifel zal ik

nooit vergeten. Ik ben blij dat wij vrienden hebben mogen worden. Opdat wij over enkele jaren een keer wél slimmer mogen zijn dan de PhD'ers (bij de pubquiz).

De warme doch werkzame sfeer op het lab kwam niet (alleen) uit de lucht gevallen. Ik ben dankbaar voor degenen om me heen in het lab, ook van de zustergroep Hensen, die mij op talloze manieren hebben geholpen: Tim, Jaimy, Koen, Lars, Sanaz, Bas, Martijn, Aaron en in het bijzonder Stef voor zijn hulp met het begrijpen van de maan.

Louw verdient een speciaal bedankje voor zijn enthousiaste verhalen over zijn tijd in de groep Oosterkamp, en voor zijn aanwezigheid op de voorpagina van mijn labjournaal.

Ik was hier in de eerste plaats nooit gekomen zonder de zogeheten PSW. Iedere PSW'er heeft individueel onmeetbaar veel voor mij betekend, vier jaar lang. Dank jullie wel: Bernard, Bryce, Charlotte, Liya, Louw, Mike, Mirte en Romme.

Een dankwoord is ook op zijn plaats aan Merlijn van de Fijn Mechanische Dienst (FMD), voor het realiseren van onze (onorthodoxe) ontwerpen, zoals het lateraal dempende blok lood (ook wel: LVIS*) en de ultra-nauwkeurig uitgelijnde massa's.

A special thank-you also goes out to Martí, who (single-handedly) fixed our COMSOL simulation during his visit, saving us time and debugging-related pain thanks to his generosity.

The warmest gratitude must naturally go to you, reader, for taking the time to read (just the acknowledgements of) this thesis. I trust it was worth your time.

This isn't even to mention how mind-bogglingly many people there are for whose presence in my life I am grateful whom I should choose not to name explicitly. There's so much to be grateful for! Who knows how many tiny things had to happen for this thesis to be written? But, as Michael Ende would say: das ist eine andere Geschichte und soll ein andermal erzählt werden.

To cut this off on a lighter note, I would like to acknowledge ChatGPT for speeding up so many parts of the research and the writing process. Generative language models are very much in their early days, but already they have proven so incredibly useful for coding, understanding and inspiring. I am still frequently amazed by ChatGPT, and overwhelmed with excitement to see what this technology can bring in the future.

Scripsi.[2]

*Lateral Vibration Isolation System; de naam is geïnspireerd door de L-vormige bladveren.

Bibliography

[1] *Wikimedia Commons*.

[2] Uitenbroek, D. (2021). Meissner Levitating Micro Particle.

[3] Van Halteren, N. T. R. (2022). Meissner Levitating Micro Particle as a gravitational force sensor.

[4] Longman, I. M. (1959). Formulas for computing the tidal accelerations due to the moon and the sun.

[5] Griffiths, D. (2017). Introduction to Electrodynamics.

[6] De Wit, M. (2019). Advances in SQUID-detected Magnetic Resonance Force Microscopy.

[7] Wijts, G. (2013). Magnetic Resonance Force Microscopy at milliKelvin [*sic*] Temperatures.